Long-term Functionality of Vacuum Insulation Panels (VIP) Subjected to Simulated Random Vibrations

By

Peng Zhan

Bachelor of Engineering, Mechanical Engineering, University of Victoria, 2021

A Thesis Submitted in Partial Fulfillment of the Requirements for the Degree of

Master of Applied Science

In the Department of Mechanical Engineering

University of Victoria

Long-term Functionality of Vacuum Insulation Panels (VIP) Subjected to Simulated Random Vibrations

By

Peng Zhan

Bachelor of Engineering, Mechanical Engineering, University of Victoria, 2021

Supervisory Committee

Dr. Phalguni Mukhopadhyaya, Co-Supervisor

Department of Civil Engineering

Dr. Caterina Valeo, Co-Supervisor

Department of Mechanical Engineering

Dr. Zhaofeng Chen, Committee Member

Department of Civil Engineering

Abstract

Due to globalization and post-pandemic developments, the shipping industry's search for energy-efficient containers in the cold chain sector has increased significantly. In this scenario, the vacuum insulation panel (VIP), a thermal superinsulation, shows significant potential to be used in the construction of highly energy-efficient shipping containers. However, a concern is a lack of information about the long-term performance of VIPs due to truck vibrations during transit.

This paper investigates this gap by presenting results from a laboratory test program involving unaged and aged VIP specimens (300 mm x 300 mm x 25 mm) with two types of core materials, fumed silica and fiberglass. The VIP specimens were subjected to random vibrations, reflecting actual in-service vibrations of a truck. Vibration tests were conducted using a Long Stroke Vibration Exciter (ball bearing type) for the low-frequency range following the procedure outlined in the ASTM Standards D4169 and D4827. Aged specimens underwent 'heat' (70 ±1°C and 5 ±3 % RH) aging in an oven and 'heat & vapour' (70 ±1°C and 95 ±3 % RH) aging in a specialized environment chamber for up to 120 days before going through random vibration tests. The change of thermal conductivity of each specimen was tracked during the random vibration test at regular intervals using a heat-flow-meter, following the procedure in the ASTM Standard C518. The results from the thermal conductivity test indicate that, in general, fumed silica VIPs have a lower degradation rate than fiberglass VIPs when subjected to simulated random vibration tests.

The findings of this study will have meaningful implications for the use of VIPs in energy-efficient refrigerated shipping containers. By identifying the impact of truck vibrations on the performance of VIPs, researchers and engineers can develop more effective methods to mitigate these effects and improve the overall integrity of the VIP-insulated highly energy-efficient

refrigerated shipping containers. Overall, this study provides insights into challenges and opportunities associated with using VIPs in the cold chain industry and opens new avenues for further research and development in this field.

Table of Contents

ABBREVIATIONS

(List in the alphabetical order)

ASD	Acceleration Spectra Density
ASTM	American Society for Testing and Materials
CO2	Carbon Dioxide
EBC	Energy in Buildings and Communities Program
FG	Vacuum Insulation Panel Specimen with Fiberglass Core Material
FS	Vacuum Insulation Panel Specimen with Fumed Silica Core Material
GHG	Greenhouse Gas
HFM	Heat-flow-meter
ICP	Integrated Circuit Piezoelectric
ISO	International Organization for Standardization
ISTA	The International Safe Transit Association
LED	Light-emitting Diode
MIL-STD	The Military Standard
Mt	Metric tons
NA	Not Applicable
ON	Ontario Province in Canada
PA	Pennsylvania State in USA
PCM	Phase Change Material
PID	Proportional, Integral, Derivative
PSD	Power Spectra Density
RH	Relative Humidity
RMS	Root Mean Square
SEM	Scanning Electron Microscope
VIP	Vacuum Insulation Panel

NOTATIONS

(List in the alphabetical order)

A	Cross-sectional Area, m^2
a	Acceleration, m/s^2
dT	Temperature Difference, K
dx	Thickness, m
E_a	Activation Energy, J/mol
f	Frequency, *Hz*
G2	Square of Gravity Acceleration, $(m/s^2)^2$
k	Dimensionless Factor
P	Gas Permeation Rate, $mol/(m^2 s Pa)$
Q	Heat Flow Rate, W/m^2
R	Gas Constant, $J/(mol \times K)$
T	Temperature, K
t	Time, hours

Greek symbols

λ	Thermal Conductivity, W/mK

List of Figures

List of Tables

Aacknowledgement

I want to express my deep appreciation to my research supervisor, Dr. Phalguni Mukhopadhyaya. Dr. Mukhopadhyaya can always point out the right path for me when I have questions during my research. I want to thank him again for his support and understanding when I encountered a sudden family health issue. Dr. Mukhopadhyaya is a great supervisor who can provide me with professional guidance and wise suggestions in my personal life. I would also like to thank Dr. Zhaofeng Chen for his wise recommendations and critical observations.

I also express my deep appreciation to my co-supervisor, Dr. Caterina Valeo. Dr. Valeo is a great professor who establishes solid connections and communication with students. I have learned much from her since my bachelor's degree at the University of Victoria.

I also like to thank the experts from CryoLogistics. Thanks for their information about insulated shipping containers.

Finally, I would like to express my deep gratitude to Mr. Bastien Lanusse, Ms. Arielle Garrett, and Dr. Armando Tura who provided tremendous assistance in the Building Science Laboratory to conduct experiments.

1. Introduction

The ongoing globalization has increased the total value of goods crossing national boundaries and contributed to higher demand in the cold chain industry. The term "cold chain" represents the transport process of perishable products under controlled temperature. Perishable products will be unsafe to use/consume if not refrigerated at appropriate temperature. The recent COVID-19 pandemic has also contributed to the growth of the cold chain industry. Proper temperature control plays a vital role during the transportation and distribution of vaccines. Grand View Research Inc. projected that the global cold chain market will reach USD 628.26 billion by the next five years with a compound annual growth rate of 14.8% from 2021 to 2028 [1]. With the rise of market value, prevention of the degradation of goods during transportation has become a very important topic. Food and Agricultural Organization (FAO) reported 13.3% food loss globally during the transportation process from supplier to end-customer in 2020 [2]. Exceeding the limited timeframe or non-professional storage are two main factors for food loss, contributing to 35% of the total food loss [3]. Findings from a case study show that transportation activities consume about 30% of the total energy required in the cold chain, and insufficient cooling contributes to 43% of product quality degradation [4]. Hence, the leading cold chain companies from all over the world are seeking innovations in various aspects, including management, packing, and storage technologies, to increase the goods' storage life and take their competitive advantages to the market [5-7].

From engineering perspective, the refrigerated container or cooling system is an essential part of the cold chain, which extends the food storage life and maintains the quality of the food. Furthermore, a refrigerated container is a good choice for transporting and distributing

temperature-sensitive products, not only fruits [8, 9] but also medicines or chemical products [10, 11]. Refrigeration technology could act as a two-edge blade, benefiting the human community while raising potential adverse environmental impacts. The main environmental footprints of refrigeration are greenhouse gas (GHG) emissions and energy use. According to the country data from the Green Cooling Initiative, the transport refrigeration sector is responsible for about 10 Mt in CO2 equivalents of direct global greenhouse gas emissions in 2022 [12]. Dong et al. [13] concluded that about 60% of total post-agriculture GHG emissions for vegetables and fruit are from refrigeration energy usage. They also reported an average of 15% ~ 19% of total post-agriculture GHG for aquatic and meat under medium temperature (-2 °C) and low temperature (-22 °C) from the same path in China. A study case of orang fruit transported from South Africa to Switzerland [14] shows that refrigeration energy usage during transportation contributes 30% ~ 42% of total GHG emissions in the cold chain. Hence, many researchers are looking at innovations in refrigeration systems for cold chains from various directions.

A refrigerated container's power consumption is mainly dominated by the automatic heat exchange between its inner and outer environment through its insulation layers. Firstly, Filina et al. [15] optimized the physical arrangements of 50 refrigeration containers' locations in a vessel to minimize the effect of natural convection between each container, and they found a reduction in average daily power consumption by 7%. Getahun et al. [16] studied the fluid dynamics of a start-of-art refrigerated container (Star cool SCI-40), and their research focuses on controlling the cooling airflow circulation inside the container to achieve a high-power efficiency of the refrigeration system in future work. Zhao et al. [17] also performed a Computational Fluid Dynamics analysis on an air-refrigerated container with a dimension of 1.5x1.5x1.6 meters, and they improved its energy efficiency by optimizing the design of air ducts and outlets.

Kayansayan et al. [18] analyzed the thermal characteristics of refrigerated containers on a moving truck, and they found the container aspect ratio (length/ height) of 3.33 provides the highest temperature distribution efficiency at half-span modeling among their experimental range of Reynolds numbers. Sengyrruvan et al. [19] also considered multiple combinations of refrigerated container geometry and its internal cooling airflow system design. The above researchers generally focus on the airflow dynamics to optimize the energy efficiency of a refrigerated container. Still, others are working on new power supplies and novel insulation material. A leading hydrogen company in France tested a refrigerated container powered by a fuel cell on a vessel [20]. Alzuwaid et al. [21] investigated the inner air temperature distribution, product temperatures, and airflow patterns of the novel refrigerated container with water gel (phase change material, in short-term "PCM") integrated. After that, other researchers studied the application of Sub-Zero Eutectic PCM solutions [22] and Rubitherm RT35HC paraffin wax [23,24] on refrigerated containers. Due to the phase-changing time delay of PCM between liquid and solid, Vacuum Insulation Panel (VIP) as a more stable insulation material attracts more attention. Multiple literature research [25, 26, 27, and 28] indicated the great potential of integrating VIP into refrigerated containers since VIP has 5~10 times higher thermal insulation performance than commercial thermal insulations [29].

Although the application of VIP as building insulation has been well investigated [30], more research on its application in refrigerated shipping containers is needed. Most current research focuses on numerical simulations of applying VIP to refrigerated shipping containers, but only a few investigated its long-term performance under specific working conditions. A refrigerated shipping container in the cold chain will be exposed to high temperature, high humidity, and constant vibration during vehicle transportation. Wernery et al. [31] performed random vibration

on VIP using pyrogenic silica core material. In Wernery's test, the simulated random vibration has a frequency range from 5 to 150 Hz, the highest amplitude at 0.532 (m/s^2) ^2/Hz, and a duration of 55 hours. The previous Wernery vibration test implemented the standard IEC 61373 "Railway applications – Rolling stock equipment – Shock and vibration tests" [32]. Kraus et al. [33] found that protecting VIP with adhesive bounding with protective material can raise its puncture resistance by a factor of five. No more publications relating to the long-term performance of VIP under random vibration were found during the literature review process. Hence, there is a missing part to solve the puzzle of the application of VIP to refrigerated shipping containers.

This research aims to provide insight into the performance change of two different core material VIPs under the simulated truck random vibration at the in-service level. This paper consists of five main sections: 1) Background: This section provides the fundamental information about Vacuum insulation panels (VIP), 'heat' and 'heat & vapour' aging of VIPs, and the vibration test of shipping containers. 2) Methodology: This section describes the methodology of the vibration test and the methodology of the two types of aging tests, including test equipment, test procedure, and data collection. The 'heat' and 'heat & vapour' aging tests were introduced first since the aged specimens for the vibration test must be explored in extreme environments for a couple of months. 3) Results: This section provides an overview of results from the vibration and aging tests. A discussion about the experimental findings is performed. For the results of the vibration test, only possible hypothesis is discussed due to the limited support of the literature review. 4) Conclusion: This section highlights the significant findings of this research. 5) Future works: This section describes the multiple directions of this experiment in the future.

2. Background

2.1 Heat Transfer Mechanisms in Vacuum Insulation Panels

Heat transfer through an object is divided into three mechanisms: convection, conduction (solid & gas) and radiation, as shown in Equation 1 below [34]. Reducing the effect of air conduction is considered the key to developing high-performance thermal insulation materials [35], and different approaches are well investigated, such as replacing air with lower thermal conductivity gas [36], reducing the pore size of insulation material to nanoscale [34,37] or reducing inner air pressure [34].

$$\lambda_{total} = \lambda_{conv} + \lambda_{solid+gas,cond} + \lambda_{rad}$$

Equation 1

Vacuum insulation panel (VIP) is a promising thermal insulating product whose working principle combines extremely low inner air pressure and high porosity core material to achieve a high thermal resistance. Gas conduction happens in still air in a thermal insulation material due to the random collision of air particles. At a sufficiently low pressure close to a vacuum, the effect of random collision of air particles is minimized. Using the high-porosity core material, evacuating air inside the thermal insulation and creating a vacuum is easier. A well-designed VIP in recent decades can provide an effective thermal conductivity of less than 0.005W/(mK) at a low inner pressure condition (generally under five millibar), which is ten times better than most conventional insulation materials. By looking at the development of VIPs over the past ten years [38,39], fumed silica and fiberglass are considered as two primary core materials to manufacture VIPs:

1. Fumed silica can provide a thermal conductivity of around 0.004W/(mK) at 20 – 100 mbar pressure. However, opacifier addition is required for fumed silica to block thermal radiation.
2. Fiberglass requires a lower vacuum pressure to achieve a thermal conductivity of around 0.002W/(mK) because of its relatively large pore size. Furthermore, the expected service life of fiberglass core VIP is somewhat lower.

Typically, manufacturers divide the VIP's envelope into three types of layers, namely the heat-sealing layers, barrier layers, and protective layers, from inside to outside:

1. The heat-sealing layer bonds the core materials.
2. The barrier layer, generally composed of aluminum foil, prevents air and water vapor penetration.
3. The protective layer handles mechanical load during transportation or installation.

In addition, the getter or desiccant is a necessary substitute for VIP products because it can absorb the moisture residual gas from vacuum residue or outside air due to the gas penetration through the VIP envelope. With the addition of a getter or desiccant, the service life of VIP can be extended.

2.2 'Heat' and 'Heat & Vapour' Aging for VIPs

EBC Annex 39 [34] reports that a high permeation rate will accelerate the degradation of VIP's thermal insulating performance in high-temperature and high-humidity environments. Core material absorbs moisture from penetrated atmospheric gas, which increases effective thermal conductivity. The penetrated atmospheric gas, primarily through the defects at the edge or wrinkle areas, also increases the inner pressure of VIP.

For polymetric material, the temperature dependence of gas permeation rate P can be estimated with temperature T, reference temperature T_{ref}, activation energy E_a, and the gas constant R in the form of the Arrhenius equation.

$$\frac{P(T)}{P(T_{ref})} = \exp\left(-\frac{E_a}{R(T-T_{ref})}\right) \quad \text{Equation 2}$$

Hence, many researchers conducted aging tests for VIPs in high-temperature and high-humidity environments. Simmler et al. [40] performed hygrothermal aging tests on several VIP products, available in Europe, under the following conditions:

- At 80℃ and 80% RH for 30 days
- At 80℃ and 80% RH for 8 hours, and then 25℃ and 50% RH for 4 hours, for 30 days
- At 30℃ and 90% RH for 150 days
- At 80℃ for 150 days

Kim et al. [41] performed an aging test on multiple fumed silica core VIP specimens with recurring temperature changes at a 12-hour interval from 80℃ to -15℃. The total test duration is 16 days, but the specimens' thermal conductivity increase is less than 10%. Several others conducted tests on VIPs focusing on different temperature and humidity levels [42,43].

This study compares the performance of fumed silica and fiberglass core VIPs after high temperature and high humidity accelerated aging tests.

2.3 Vibration Test of a Shipping Container

Multiple research projects on different road conditions, from different nations, measured the truck vibration in the vertical direction, while in service [44-47]. The truck vibration is usually characterized by truck suspension systems: 'air-ride' or 'steel-spring'. The random vibration

profile is defined by a set of frequency and amplitude breakpoints. Equation 3 describes the vibration intensity level as acceleration root mean square (RMS).

$$Acceleration\ RMS = \sqrt{\int_{f_1}^{f_2} a(f) * df}$$

Equation 3

Where, $a(f)$ is the recorded acceleration in $(m/s^2)^2/Hz$ at a specific frequency instant, f_1 is the first frequency instant *Hz*, and f_2 is the last frequency instant in *Hz*. Therefore, Acceleration RMS has unit as (m/s^2).

Chonhenchob et al. [44] reported that the truck vibration level in Thailand has a range of acceleration RMS from 1.83 to 3.53 (m/s^2) and a typical frequency range from 1 to 100 *Hz*. Zhou et al. [45] reported that, in China, the vibration level for a standard load truck has an acceleration RMS from 1.57 to 2.45 (m/s^2) at a frequency range from 1 to 200 *Hz*, and the vibration level for an overloaded truck has an acceleration RMS from 0.39 to 2.16 (m/s^2) at the same frequency range. Garrido et al. [46] reported that the truck vibration level in Spain has an acceleration RMS from 0.78 to 2.45 (m/s^2) at a frequency range from 1 to 100 *Hz* by summarizing data from 30 routes. The truck vibration on the North American road was measured by Singh et al. [47], and their results show an acceleration RMS from 0.59 to 3.63 (m/s^2) for the lower 70% recorded data but an acceleration RMS from 0.98 to 8.73 (m/s^2) for the high 30% recorded data. One significant finding in this study was that a route from Carlisle (PA) in the USA to Hawkesbury (ON) in Canada had only a 0.69 (m/s^2) acceleration RMS at low 70% recorded data and 1.27 (m/s^2) acceleration RMS at high 30% recorded data.

Several global standards are available for vibration tests of shipping containers:

- *ASTM D4169 Standard Practice for Performance Testing of Shipping Containers and Systems*: Provides different test guidelines for a shipping container, and 'Schedule E-Vehicle Vibration' provides acceleration spectral density (ASD) profile to simulate the actual truck transport vibration environment [48].
- *ASTM D4728 Standard Test Method for Random Vibration Testing of Shipping Containers*: Covers the random vibration test procedure for a shipping container to assess its performance [49].
- *ISTA 3H Products or Packaged-Products in Mechanically Handled Bulk Transport Containers*: 'Sequence 8 Random Vibration' covers the testing procedure for one transport container or system consisting of the same product that, because of their size/weight, must be transported by truck or rail [50].
- *ISO 13355 Packaging – Complete, filled transport packages and unit loads – Vertical random vibration test*: Covers a method to carry out a vertical random vibration test on complete, filled transport package(s) and unit loads using a random excitation [51].
- *MIL-STD-810-G Environmental engineering considerations and laboratory tests*: Method 514.6 'Annex C Transportation Tailoring Guidance for Vibration Exposure Definition' covers information on transportation environments that is intended to help determine the vibration levels and durations of environmental life cycle events and defines the tests necessary to develop material to operate in and survive these environments [52].

All the above standards [48-52] suggest specific random vibration profiles for truck vertical vibration. Still, there are minor differences among those vibration profiles and test requirements. For civilian application random vibration test is mostly considered on only vertical axis [48-51],

while for military applications vibrations on transverse and longitudinal axis are considered [52]. Report from various research about truck vibration data in different nations [44-47] demonstrate the vibration energy level on the vertical axis is larger than that on transverse or longitudinal axis. Table 1 shows the significant elements of truck random vibration in each standard mentioned above, while 'ASD' stands for acceleration spectra density.

Table 1: Truck random vibration test key element in each global standard.

Truck Vibration ASD	Truck Suspension type	Level	Direction	Frequency [*Hz*]	Acceleration RMS [*m/s^2*]	Duration	Number of Breakpoints
ASTM D4169/4728	NA	High	Vertical	1-200	6.87	Until Damage Detected	12
		Medium			5.29		
		Low			3.92		
ISTA 3H	Steel Spring	NA	Vertical	1-200	5.29	4 Hours Max.	12
	Air Ride			0.6-100	2.75		9
ISO13355	NA	NA	Vertical	2-200	5.93	30min Min.	5
MIL-STD 810-G	NA	NA	Vertical	10-500	10.2	Not Defined	3
			Transverse		1.96		7
			Longitudinal		7.26		8

All the acceleration RMS in Table 1 are more intensive than all the lower limits of truck vibration in service from literature reviews [44-47]. Even considering the high limit of truck vibration in service, the acceleration RMS in Table 1 has still been scaled up by certain factors. The figures below show two examples of vibration profiles to explain the difference in detail. Figure 1 and Figure 2 share the feature having the most significant intensities during the same frequency range, but Figure 1 has the higher order of general energy level. The term 'PSD' stands for power spectra density, which is the equivalent of acceleration spectra density in vibration. The unit 'G2' in Figure 1 and 2 is the square of gravity acceleration in $(m/s^2)^2$.

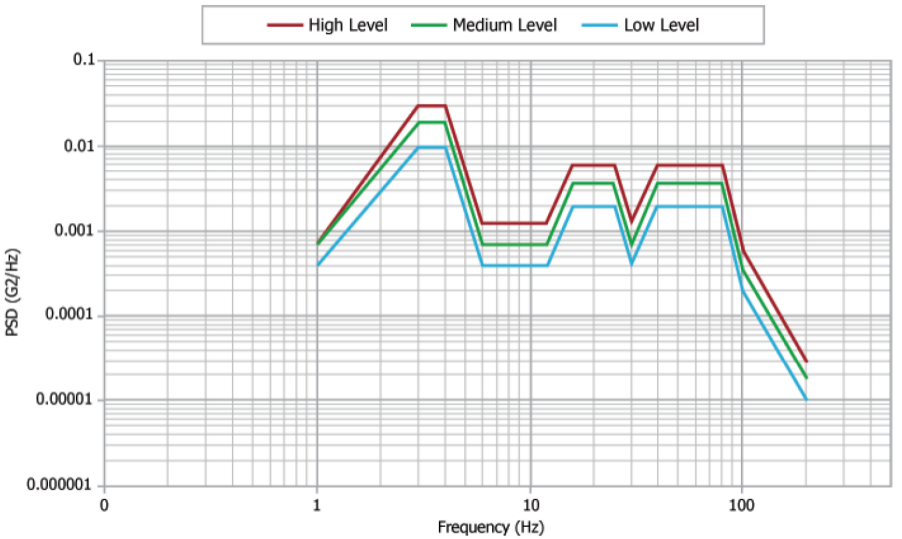

Figure 1: Power spectra density profile from ASTM standard D4169.

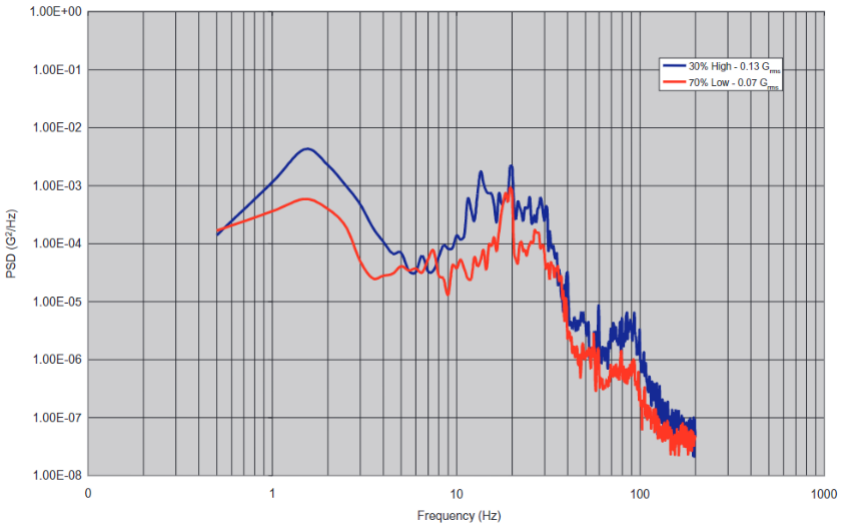

Figure 2: The recorded air-ride truck PSD profile of trip from Carlisle to Hawkesbury [47].

Shires (2011) explains that the global standard accommodates the time compression method for accelerated random vibration test, based on '*Miner – Palmgren hypothesis*', as shown in equation 4 [53].

$$\frac{t_{test}}{t_{in\,service}} = \left(\frac{a_{in\,service}}{a_{test}}\right)^{k} \qquad \text{Equation 4}$$

Where, t_{test} is the test duration, $t_{in\,service}$ is the equivalent duration in service, a_{test} is the acceleration RMS in test, $a_{in\,service}$ is the acceleration RMS in service, and k is a constant. Furthermore, the number of breakpoints in Table 1 represents the comprehensiveness of the suggested random vibration profile, which means how many significant frequency instants are introduced.

2.4 Thermal Conductivity Measurement of VIP

In recent years, methods for thermal conductivity measurement have been divided into steady-state and transient methods. The steady-state method, based on Fourier's Law, Equation 5, has a higher accuracy but a longer testing time required than the transient method [54].

$$Q = -\lambda A \frac{dT}{dx} \qquad \text{Equation 5}$$

Where Q is the heat flow rate of thermal conduction, λ is the thermal conductivity of the specimen, A is the cross-sectional area of the specimen, dT is the temperature difference between the specimen's surfaces, and dx is the thickness of the specimen.

In this study, heat-flow-meter apparatus is used for steady-state thermal conductivity measurements. The working principle of the heat-flow-meter method is simply establishing the steady-state of one-dimensional heat flux through a specimen between two parallel plates at

constant temperature gradient. This test is guided by the ASTM C518 - Standard Test Method for Steady-State Thermal Transmission Properties by Means of the Heat-flow-meter Apparatus [55].

3. Methodology

3.1 VIP Specimens

Two types of Vacuum Insulation Panels (VIPs) were considered in this study: (i) fumed silica core VIPs and (ii) fiberglass core VIPs (both 300 mm x 300 mm x 25 mm). In total, 24 VIP specimens were considered. 12 fumed silica VIP specimens were labelled as FS1 to FS12, and 12 fiberglass VIP specimens were labelled as FG1 to FG12. Six (6) VIP specimens (Fumed silica: FS1, FS2 and FS3; Fiberglass: FG1, FG2 and FG3) were assigned as control panels, storing at the laboratory condition (22±1°C, 45±5% RH). Table 2 below shows the specifications of the tested specimens provided by manufacturers [56,57]. Figure 3 shows the fumed silica specimen and fiberglass specimen.

Table 2: Specifications of two type specimens.

Core type	Density [kg/m^3]	Thermal conductivity [W/mk]	Internal pressure	Temperature range [°C]	Component	Compressive strength
Fumed silica	160-190	0.0037@ 1mbar 0.019 @ ambient pressure	≤ 5 mbar	-50 ≤T≤120	Outer bag: metalized, multilayer plastic film Opacifier: No detail	100kPa @10%
Fiberglass, glass wool	223	0.002	No detail	-40≤T≤60	Outer bag: laminated plastic film with aluminum Desiccant: Calcium Oxide Air absorbent: Zeolite	98.6 kPa @25%

Figure 3(a): Fumed silica specimen.

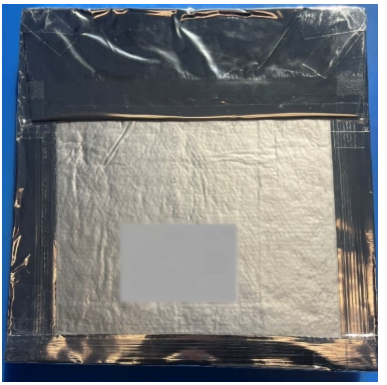

Figure 3(b): Fiberglass specimen.

3.2 'Heat' and 'Heat & Vapour' Aging of VIPs

Six (6) fumed silica VIP specimens (FS4 to FS9) and six (6) fiberglass VIP specimens (FG4 to FG9) were used for the 'heat' and 'heat & vapour' aging tests. The duration of aging tests was up to 120 days. Two environmental conditions were:

Condition 1: Constant 70 ±1℃ temperature and 5±3% RH, and

1. Condition 2: 70±1℃ temperature and 95±3% RH.

The VWR gravity convection oven in Figure 4, operating at a temperature range of 50 to 250℃, with automatic temperature control, was used to achieve Condition 1 above. The fumed silica VIP specimens (FS4, FS5 and FS6) and the fiberglass VIP specimens (FG4, FG5 and FG6) were subjected to 'heat' aging in the oven.

Figure 4(a): VWR Oven used for 'heat' aging. *Figure 4(b): Inner view of VWR Oven.*

A customized environmental chamber (Figure 5) was used to achieve Condition 2. The chamber consists of a well-sealed tank with a certain amount of water inside, a heating pad attached to the bottom of the tank, a thermocouple placed inside the tank for temperature control, an INKBIRD thermal PID controller, and a large outer box isolating the inside condition from the ambient condition. The fumed silica VIP specimens (FS7, FS8 and FS9) and the fiberglass VIP specimens (FG7, FG8 and FG9) were subjected to the 'heat & vapour' aging test in this chamber.

Figure 5(a) shows the outer view of the environmental chamber used for 'heat & vapour' aging tests and Figure 5(b) shows the inner view of the same. Figure 5(c) shows the heating control unit with a LED display. Initially, the thermal conductivities of twelve specimens were measured every five days. However, thereafter the measurements were taken at every ten days.

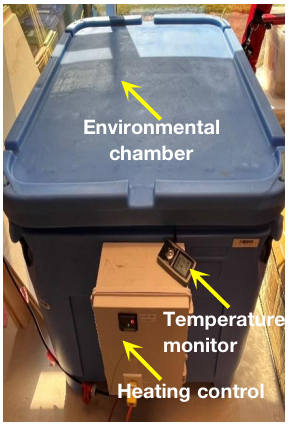

Figure 5(a): Customized environmental chamber for 'heat & vapour 'aging.

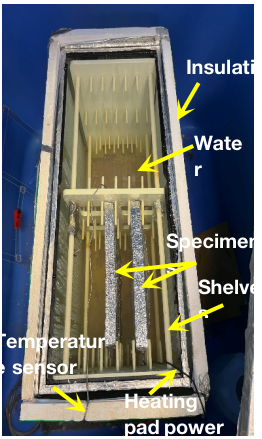

Figure 5(b): Inner view of environmental chamber.

Figure 5(c): Inkbird thermal control box.

3.3 Random Vibration Test

The applicability of an elevated acceleration spectra density (ASD) profile is adopted in this study for random vibration tests because the applicability of fatigue models for packaging tests are not well-investigated yet [53]. Wang et al. [58] concluded that the elevated ASD method is only valid for linear packaging systems under specific assumptions. The vibration damage and fatigue models are different for different materials due to the damage mechanism in different materials, and the components of the packaging container are also different. Since the vibration fatigue model for VIPs has not been established yet, the applicability of the elevated ASD test to VIPs is questionable. Hence, in this study a scaled-down ASD profile from the ASTM Standard D4169 was used to simulate the lower limit of truck vibration level in service.

The chosen ASD profile is the truck random vibration profile (high-level) from the ASTM D4169 [48] because Table 2 shows that ASTM D4169 is more comprehensive at simulating the

truck vibration environment in service; it includes more breakpoints than the other standards during similar frequency range. Figure 6 below illustrates the scaled-down ASD profile for the vibration test, with a targeted acceleration RMS at 0.6975 m/s^2.

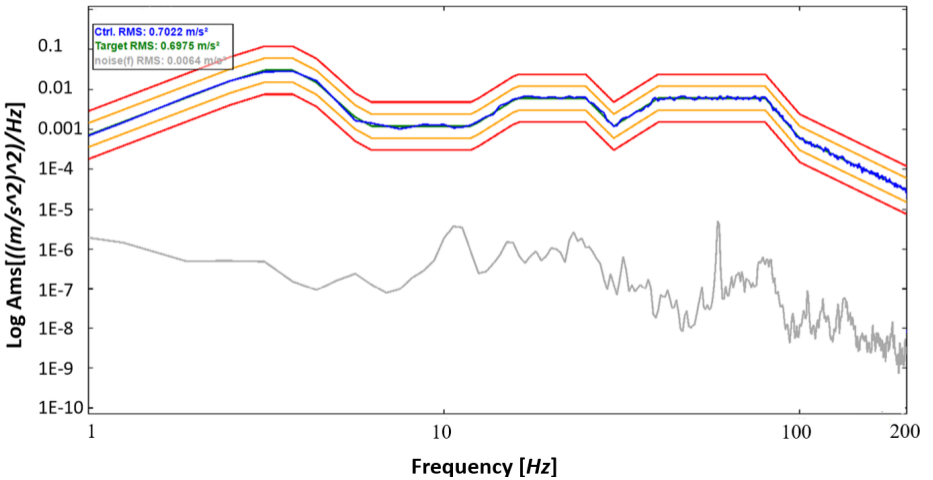

Figure 6: Modified ASD profile in the test.

Three unaged fumed silica VIP specimens (labelled FS10, FS11, FS12) and three unaged fiberglass VIP specimens (labelled FG10, FG11, FG12) were considered for the truck random vibration tests. Six aged VIP specimens (Fumed silica: FS4, FS6 and FS7; Fiberglass: FG4, FG5, and FG8) from 'heat & vapor' aging tests were also experimented with random vibration for 120 hours. Table 3 below describes the details of the random vibration tests. In the vertical orientation of the specimen, 'Constrained' represents that the specimen was fixed on the shaking table, and its vibration level was assumed to be the same as the shaker output level. 'Free' means two soft foam layers held one specimen in position, and its vibration level is lower than the targeted level since the two soft foam layers act as dampers in this system. The 'Free' and

'Constrained' cases simulate the VIP-integrated side walls of a shipping container with two different arrangements. In the horizontal orientation of the specimen, the specimen was constrained on the shaking table at the horizontal plane, and a 14kPa load was applied at three chosen locations on the specimen's top surface (See Figure 10). Due to the capacity limit of the vibration system, used in this study, a uniform load across the specimen's top surface could not be applied. This case simulates the VIP-integrated bottom of a shipping container under loads. After every single test cycle of 24 or 48 hours, the specimens' weight and thermal conductivity were recorded for further analysis.

Table 3: Random vibration test schedule.

ID	Condition	Aging type	Core material	Specimen Orientation	Test Type	Test Hours
FS1	Control	NA	Fumed silica	NA	NA	0
FS2						0
FS3						0
FG1			Fiberglass			0
FG2						0
FG3						0
FS5	Aged	'Heat'	Fumed silica	NA	Not subject to vibration test since failure happened in aging process	0
FS8		'Heat&Vapor'				0
FS9						0
FG6		'Heat'	Fiberglass			0
FG7		'Heat&Vapor'				0
FG9						0
FS6	Aged	'Heat'	Fumed silica	Vertical	Constrained	120
FS7		'Heat&Vapor'				120
FS4		'Heat'		Horizontal	Loaded	120
FG4		'Heat'	Fiberglass	Vertical	Constrained	120
FG8		'Heat&Vapor'				120
FG5		'Heat'		Horizontal	Loaded	120
FS10	Unaged	NA	Fumed silica	Vertical	Constrained	480
FS11					Free	480
FS12				Horizontal	Loaded	480
FG10			Fiberglass	Vertical	Constrained	480
FG11					Free	480
FG12				Horizontal	Loaded	480

The vibration system consists of an APS 400 ELECTRO-SEIS long-stroke shaker (Figure 7(a)), and APS 145 power amplifier (Figure 7(b)), a Spider 81B vibration controller (Figure 7(b)), and two ICP accelerometers ((Figures 7(c) and 7(d)). The control logarithm is closed-loop control, which simultaneously adjusts output voltage according to the feedback from accelerometers. The equipment used for the simulated random vibration test is shown in Figure 7.

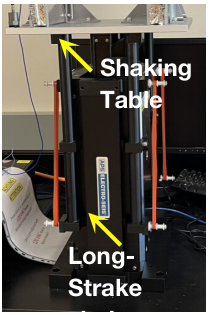

Figure 7(a): APS long-stroke shaker.

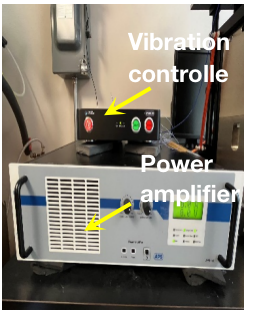

Figure 7(b): APS amplifier and Crystal Instruments vibration controller Spider 81B.

Figure 7(c): PCB 352A24 accelerometer .

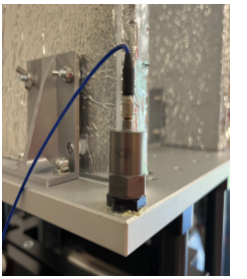

Figure 7(d): PCB 353B34 accelerometer.

Figure 7(c) shows the accelerometer mounting on the specimen to record the accelerations during the vibration test; 7(d) shows the accelerometer mounting on the shaking table for completing the closed-loop control during the vibration test.

A schematic graph in Figure 8 below demonstrates the working principle of this vibration test. A vibration control software sends out the control signal according to the input parameters

(frequency and amplitude). The accelerometer sends back the feedback signal, which closes this control loop.

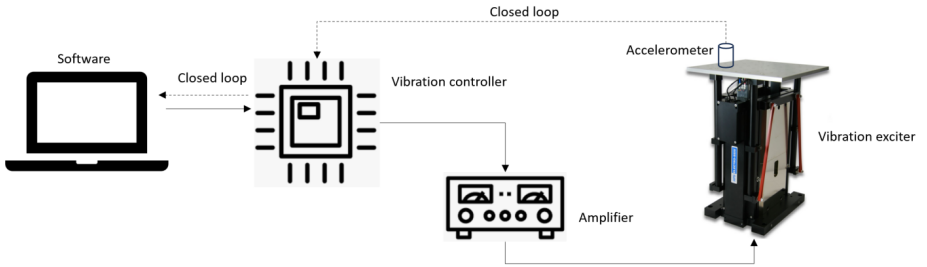

Figure 8: Schematic graph of vibration test in this experiment.

Figure 9 below shows the apparatus set-up for the simulated vertical random vibration test. The specimen on the left is constrained during the vibration ('Constrained' in Table 3), and the specimen on the right has certain freedom ('Free' in Table 3).

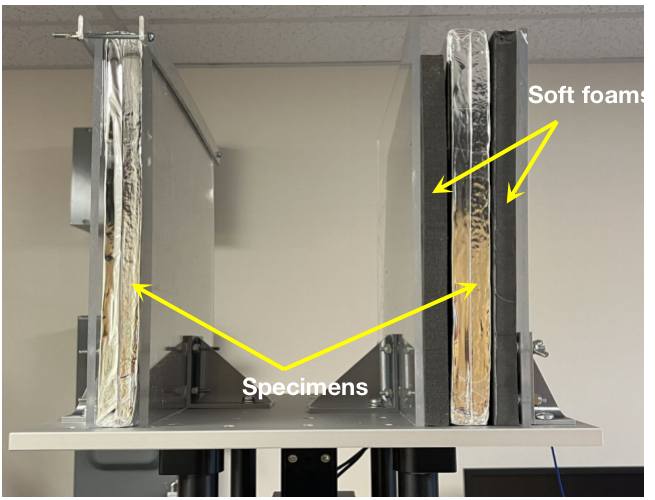

Figure 9: Testing apparatus set-up for the simulated random vibration test at specimen vertical orientation.

In the simulated horizontal vibration test, the load is applied to three locations on the specimen's surface: the rectangular boxes in Figure 10. Figure 11 shows the test set-up for the vibration test on a VIP specimen horizontal orientation with 14kPa load ('Loaded' in Table 3).

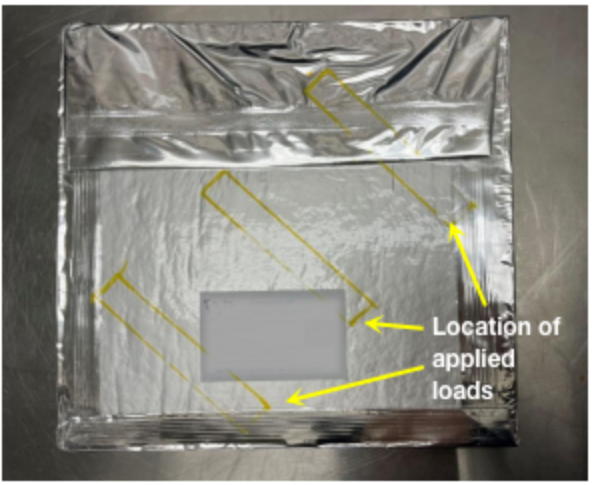

Figure *10*: Load applying location on specimen surface.

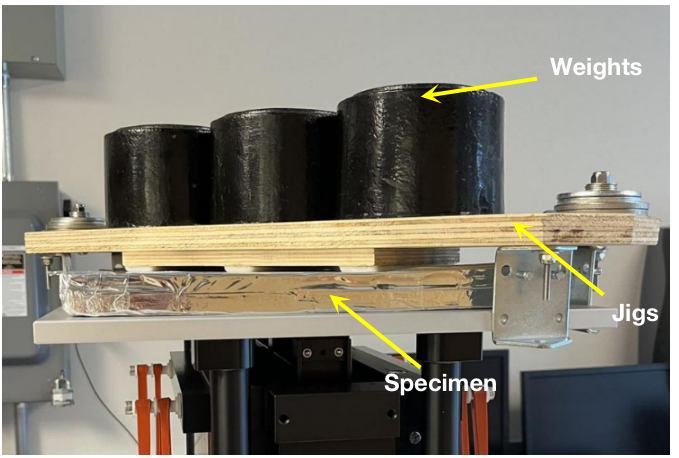

Figure 11: Testing apparatus set-up for the simulated random vibration test at specimen horizontal orientation with load.

3.4 Thermal Conductivity Measurement

The thermal conductivity of specimens was measured after each test cycle, according to the procedure outlined in the ASTM Standard C518 [55]. All specimens were reconditioned at the laboratory condition (22±1 ° C, 45±5% RH) for 24 hours before the measurement. The test apparatus is a heat-flow-meter (HFM) (NETZSCH 436 Lambda), and this equipment has an accuracy of 1~3%. The data were collected at a mean temperature of 10 ℃, and the temperature gradient between the cold and hot surfaces was 20 ℃. The data from the HFM test were updated at one (1) minute interval, the fine block size is 10 points, and the maximum fine error is 0.5%. In other words, a successful result was obtained when the last 10 data points of the specimen's thermal conductivity fell within 0.5% of the mean value of those 10 points. However, due to the specimens' very low thermal conductivity, the measurement often took hours and even days to reach thermal equilibrium. Hence, the average value of the last hour readings for specimens measured for more than 8 hours was considered a reliable measure of its thermal conductivity. Figure 12(a) shows the heat-flow-meter used for specimen's thermal conductivity measurement, and Figure 12(b) shows the cooling system attached to the heat-flow-meter for the purpose of circulating the heat flow.

Figure 12(a): NETZSCH heat-flow-meter.

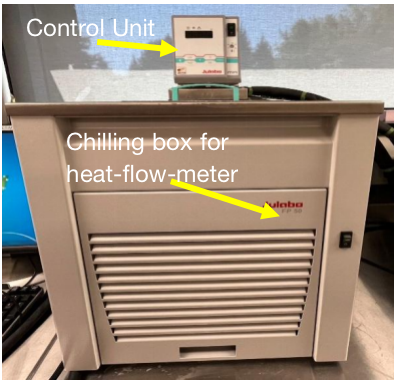

Figure 12(b): Chilling system for heat-flow-meter.

4. Results and Discussion

4.1 Results from 'Heat' and 'Heat & Vapour' Aging

The recorded change of thermal conductivity and weight for fumed silica VIP specimens ('heat' aging: FS4, FS5 and FS6; 'heat & vapour' aging: FS7, FS8 and FS9) subjected to aging test for up to 120 days are shown in Section 4.1.1. The recorded change of thermal conductivity and weight for fiberglass VIP specimens ('heat' aging: FG4, FG5 and FG6; 'heat & vapour' aging: FG7, FG8 and FG9) subjected to aging test for up to 100 days are shown in Section 4.1.2.

4.1.1 Fumed silica specimens

The recorded thermal conductivity and percentage change of fumed silica VIP specimens (FS4-9) are shown in Figure 13 and Figure 14. The percentage change is calculated from dividing the difference between specimen's thermal conductivity measurement and its initial value by its initial value. 200% increase of a VIP's initial value is normally considered as a failure, and the vacuum condition lost of a VIP is also considered as a failure. The fumed silica VIP specimen

FS8 suddenly changed after day 80, while the thermal conductivity of fumed silica VIP specimens FS7 and FS9 increased consistently starting from the beginning of the 'heat & vapour' aging test. Based on the technical datasheet (Appendix I, [56]) of the fumed silica VIP product, its thermal conductivity will reach about 450% of its initial value at ambient pressure. Thus, results indicate that fumed silica VIP specimen FS8 lost its inner vacuum condition (i.e. failed). However, the linear best-fit line in Figure 13(b) represents the aging pattern with errors, based on the average results obtained from specimens FS7, FS8 (pre failure) and FS9. The possible sources of errors are the accuracy of testing apparatus (3%) and random errors due to the moisture fluctuation during the measurement.

The change of thermal conductivity data recorded for the fumed silica VIP specimens (FS4, FS5, and FS6) subjected to 'heat' aging test are shown in Figure 13. Hence, the aging pattern for those three specimens is also obtained by finding the linear best-fit trendline of their averaged values shown in Figure 13(c).

In Figure 13(a), the data of fumed silica VIP specimens FS7, FS8 and FS9 were plotted according to the left vertical axis; while the data of fumed silica VIP specimens FS4, FS5, and FS6 were plotted according to the right vertical axis.

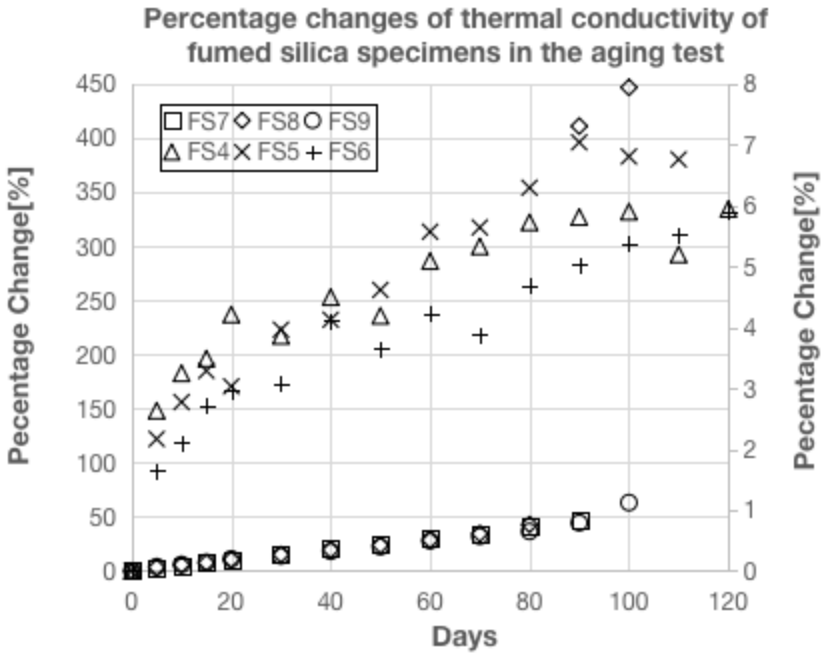

Figure 13(a): Plot of percentage changes of thermal conductivity of fumed silica specimens in aging test.

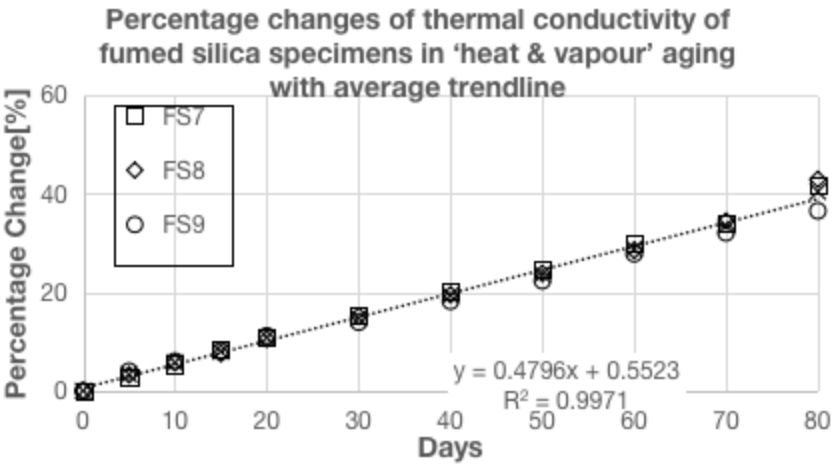

Figure 13(b): Plot of percentage changes of thermal conductivity of fumed silica specimens in 'heat & vapour' aging with average trendline.

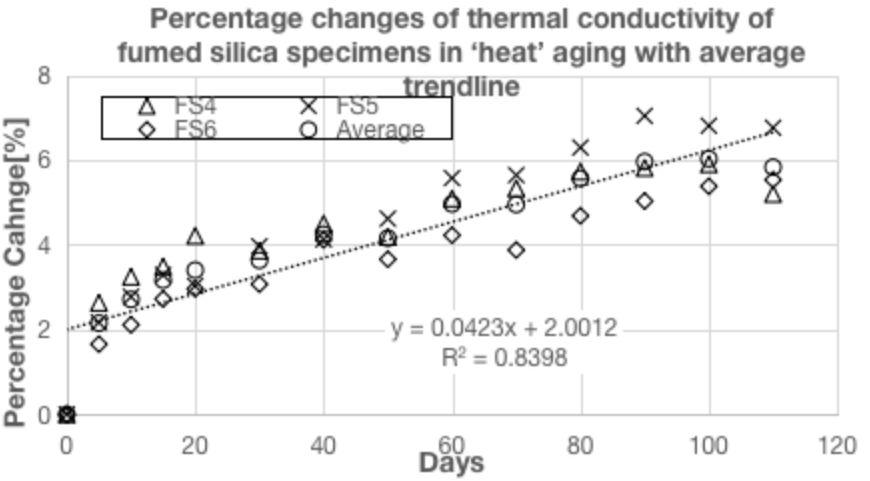

Figure 13(c): Plot of percentage changes of thermal conductivity of fumed silica specimens in 'heat' aging with average trendline.

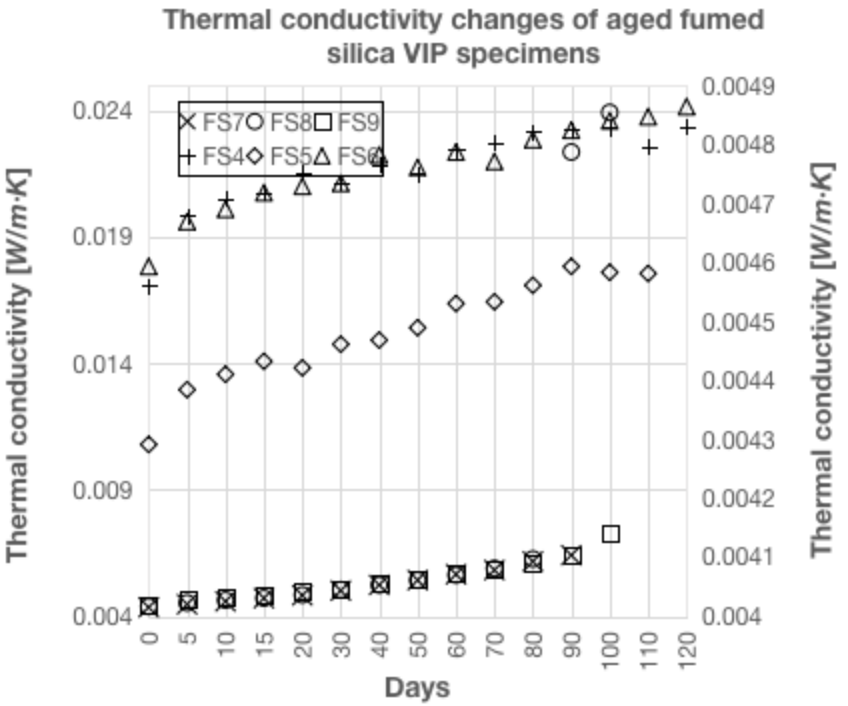

Figure 14: Plot of thermal conductivity changes of aged fumed silica VIP specimens.

In Figure 14, the data of fumed silica VIP specimens FS7, FS8 and FS9 were plotted according to the left vertical axis; while the data of fumed silica VIP specimens FS4, FS5, and FS6 were plotted according to the right vertical axis.

Figure 15 below shows the weight change of fumed silica VIP specimens during aging tests ('heat' and 'heat & vapour').

The weight changes of fumed silica VIP specimens (FS4, FS5, and FS6) are small to be negligible, so the weight change pattern of fumed silica specimen in the 'heat & vapour' aging test can be obtained by finding the linear best-fit trendline of the averaged values from fumed silica VIP specimens FS7, FS8, and FS9 shown in Figure 15(b). The possible sources of errors are the balance accuracy and human errors when reading specimen's weights.

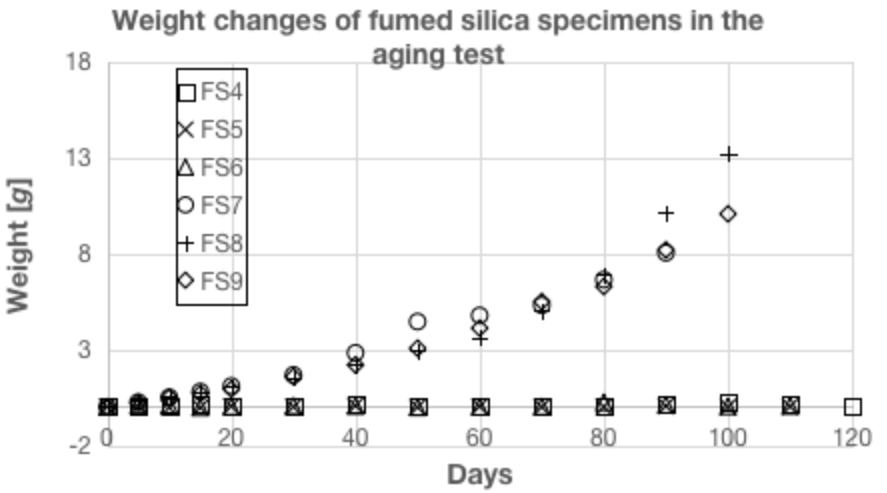

Figure 15(a): Plot of weight changes of fumed silica specimens in the aging tests.

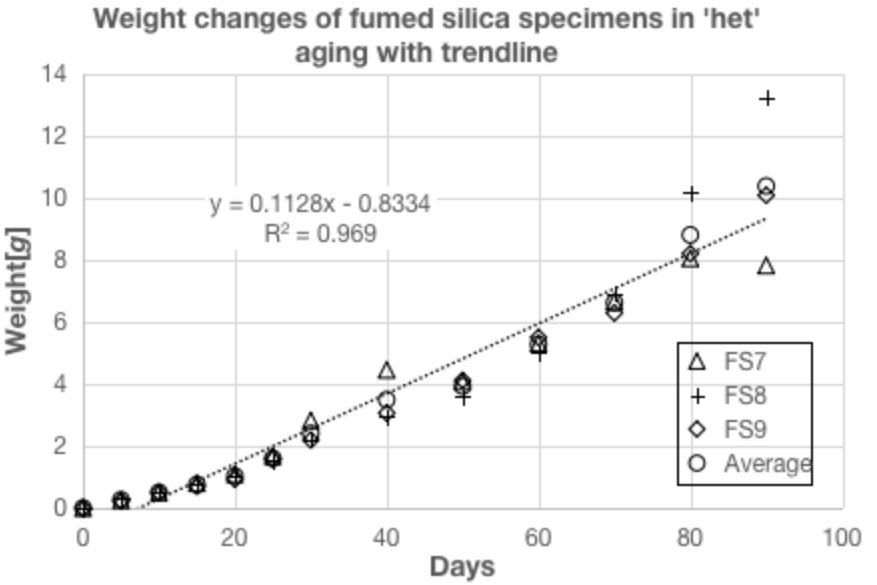

Figure 15(b): Plot of weight changes of fumed silica specimens in 'heat' aging with trendline.

4.1.2 Fiberglass specimens

The recorded thermal conductivity and percentage change of the fiberglass specimens ('heat' aging: FG4, FG5 and FG6; 'heat & vapour' aging: FG7, FG8 and FG9) are shown in Figure 16 and Figure 17. In Figure 16(a), the data of fiberglass VIP specimens FG7, FG8 and FG9 were plotted according to the left vertical axis; while the data of fiberglass VIP specimens FG4, FG5, and FG6 were plotted according to the right vertical axis. The percentage change is calculated from dividing the difference between specimen's thermal conductivity measurement and its initial value by its initial value. The fiberglass VIP specimens had different behaviours ('heat' aging: FG4, FG5 and FG6; 'heat & vapour' aging: FG7, FG8 and FG9) in the aging test compared with that of fumed silica VIP specimens in Figure 14. Those six (6) fiberglass

specimens had almost the same behavior before 60 days. However, after 60 days of the aging test the thermal conductivities of fiberglass VIP specimens (FG7, FG8, and FG9) in 'heat & vapour' aging ramped up quickly to failure. EBC Annex 39 [34] pointed out that fiberglass core VIP has a failed thermal conductivity of 35-40 $\times 10^{-3} W/(mK)$ at ambient pressure, representing the 1250% - 1400% increase in thermal conductivity of the chosen fiberglass VIP specimens in this study. The aging pattern of fiberglass VIP specimens (FG4, FG5, and FG6) in 'heat' aging can be obtained by finding the linear best-fit trendline of their averaged values, as shown in Figure 16(b). The possible sources of errors are the accuracy of testing apparatus (3%) and random errors due to the moisture fluctuation during the measurement.

To analyze the aging pattern of fiberglass VIP specimens (FG7, FG8, and FG9) in 'heat & vapour' aging, Figure 16 was modified, as described below.

The first step of the modification is averaging the two sets of fiberglass VIP specimens individually (see Figure 18), where the term 'Average 1' stands for the average value of fiberglass VIP specimens (FG4, FG5, and FG6) in 'heat' aging but the term 'Average 2' stands for the average value of fiberglass VIP specimens (FG7, FG8, and FG9) in 'heat & vapour' aging.

The difference is more apparent in Figure 18. Before day 60, the fiberglass VIP specimens can still handle the extra moisture load in 'heat & vapour' aging. Hence, the second step is isolating the two sections (before day 60 and after day 60) from the plot (see Figure 19).

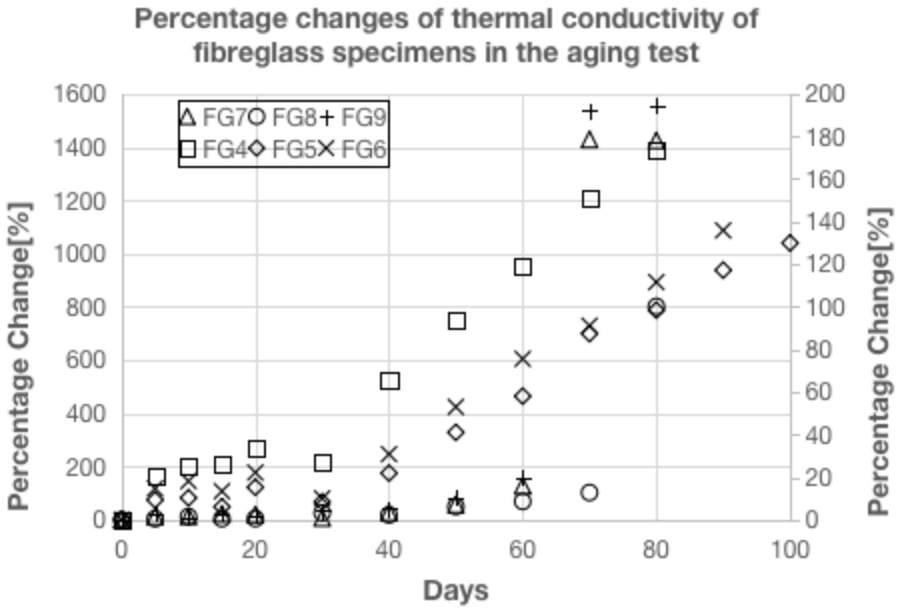

Figure 16(a): Plot of percentage changes of thermal conductivity changes of fiberglass specimens in the aging test.

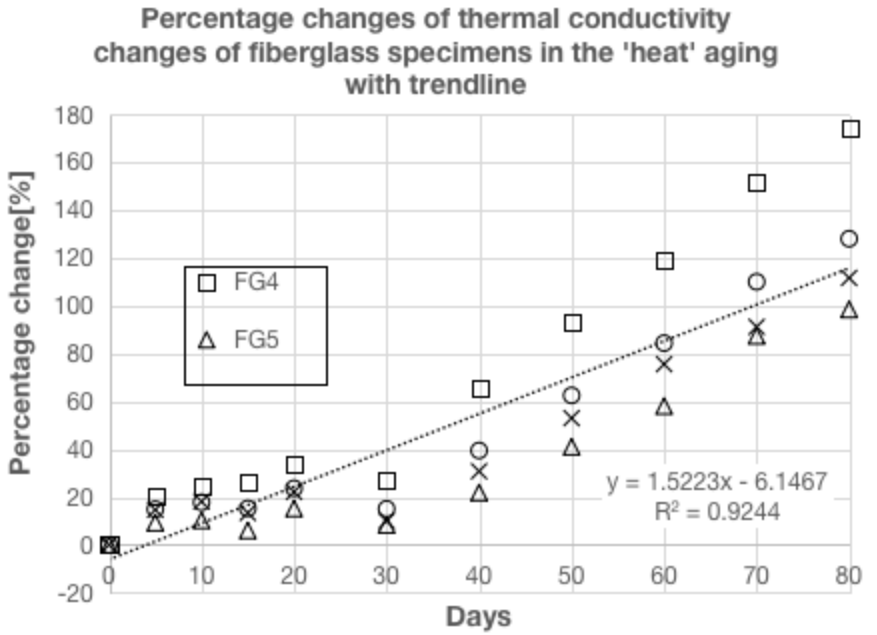

Figure 16(b): Plot of percentage changes of thermal conductivity changes of fiberglass specimens in the 'heat' aging with trendline.

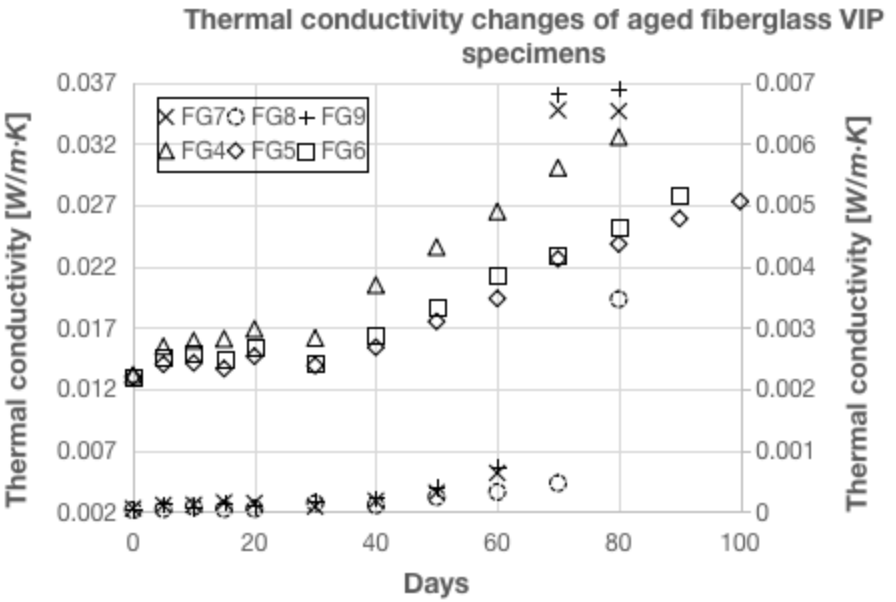

Figure 17: Plot of thermal conductivity changes of aged fiberglass VIP specimens.

In Figure 17, the data of fiberglass VIP specimens FG7, FG8 and FG9 were plotted according to the left vertical axis; while the data of fiberglass VIP specimens FG4, FG5, and FG6 were plotted according to the right vertical axis.

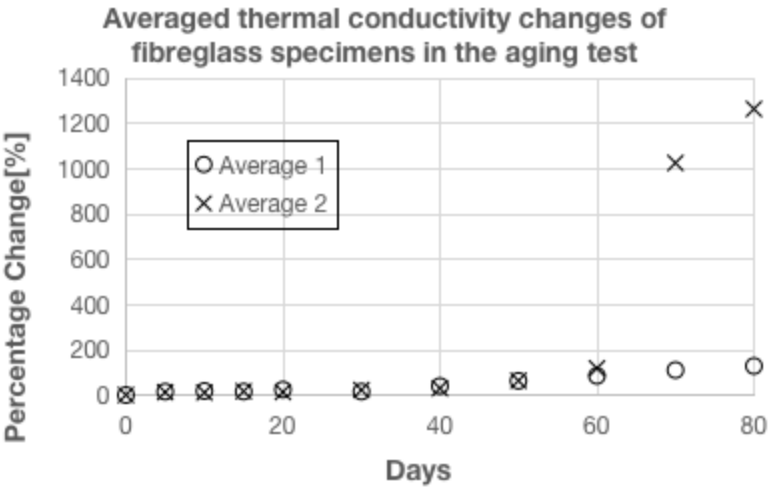

Figure 18: Plot of averaged thermal conductivity changes of fiberglass specimens in the aging test.

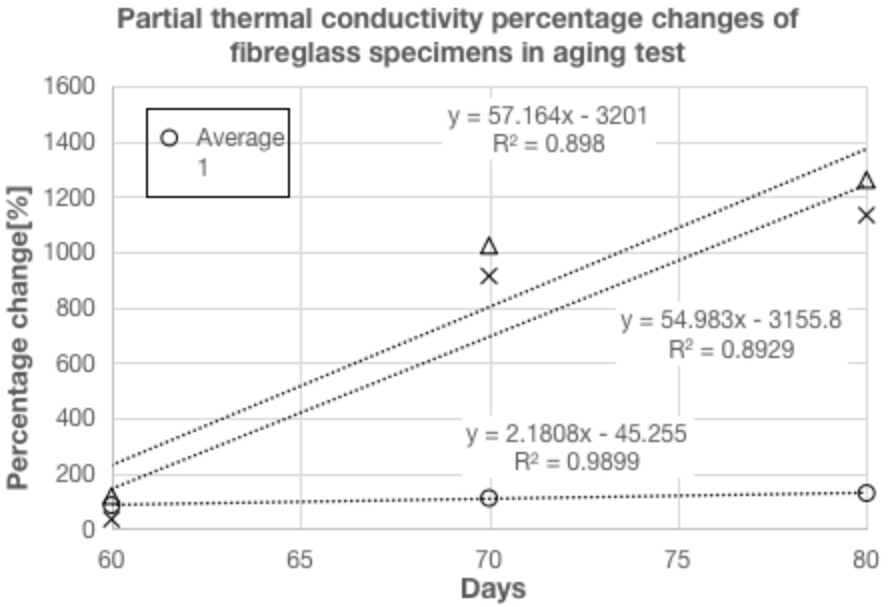

Figure 19: Plot of partial thermal conductivity percentage changes of fiberglass specimens in the aging test.

The difference between the two trendlines in Figure 19 represents the aging pattern of fiberglass specimens in pure water vapor aging (after day 60), Data point named as 'Vapor' in Figure 19 is the difference from the subtraction (subtract data of 'heat' aging from data of 'heat & vapour' aging). The linear best-fit trend of vapor shows the aging pattern of pure water vapor in Figure 19.

Figure 20 shows the recorded weight change of fiberglass specimens ('heat' aging: FG4, FG5 and FG6; 'heat & vapour' aging: FG7, FG8 and FG9) in the aging test. However, the weight changes of fiberglass VIP specimens in 'heat' aging (FG4, FG5, and FG6) are small to be negligible. Therefore, the weight change pattern of fiberglass VIP specimens in water vapor

aging is derived by finding the linear best-fit trendline of the averaged value of VIP specimens FG7, FG8, and FG9, shown in Figure 20(b). The possible errors related to the balance accuracy and human errors when reading specimen's weights.

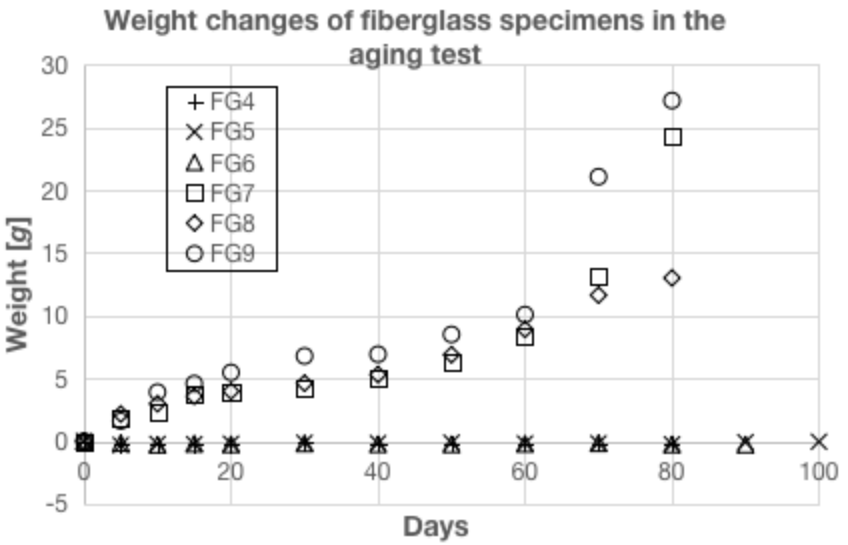

Figure 20(a): Plot of weight changes of fiberglass specimens in the aging test.

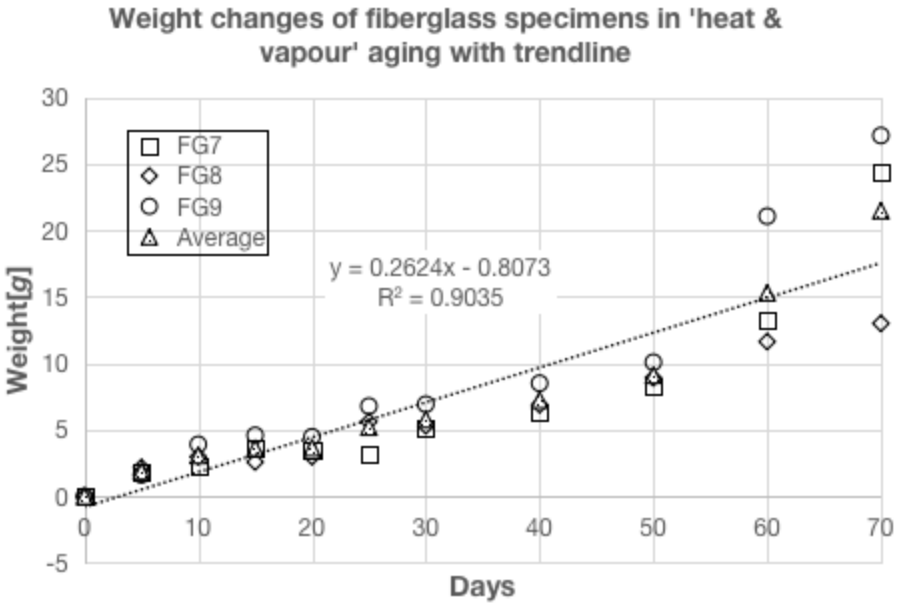

Figure 20(b): Plot of weight changes of fiberglass specimens in 'heat & vapour' aging with trendline.

For the comparison between the aging behaviours of two different core material Vacuum Insulation Panels (Fumed silica and Fiberglass), Figure 21 combines the weight change of fumed silica VIP specimens (in Figure 15) and of fiberglass VIP specimens (in Figure 20).

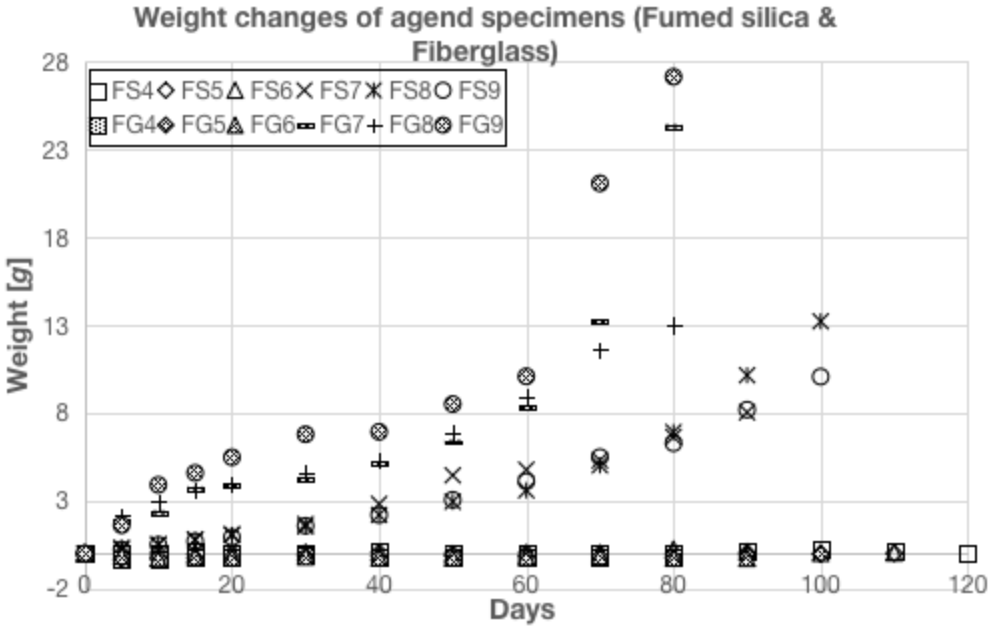

Figure 21: Weight changes of aged specimens (Fumed silica & fiberglass).

The difference of weight change between fumed silica VIP specimens (FS4, FS5 and FS6) and fiberglass VIP specimens (FG4, FG5 and FG6) in 'heat' aging is small. However, the difference of weight change between those two types of specimens in 'heat & vapour' aging is obvious in Figure 21 starting from the day 10. The average weight change of fiberglass VIP specimens (FG7, FG8 and FG9) at the end of 'heat & vapour' aging test was 21.5 grams, while the average weight change of fumed silica VIP specimens (FS7, FS8 and FS9) at the end of 'heat & vapour' aging test was 10.37 grams. It is concluded that more moisture was absorbed by fiberglass, desiccant and getter in fiberglass VIP specimens in 'heat & vapour' aging test. In other words, fumed silica VIP specimens have better performance to resist the moisture permeation from outside in a high temperature and high humidity environment.

Weight change of Vacuum Insulation Panels is one evidence of their thermal conductivity increasement, and the change of VIP's inner pressure is also related to the change of its thermal conductivity. The relationship between VIP's inner pressure changes and their thermal conductivity change is well investigated [59] and shown in Figure 22 below.

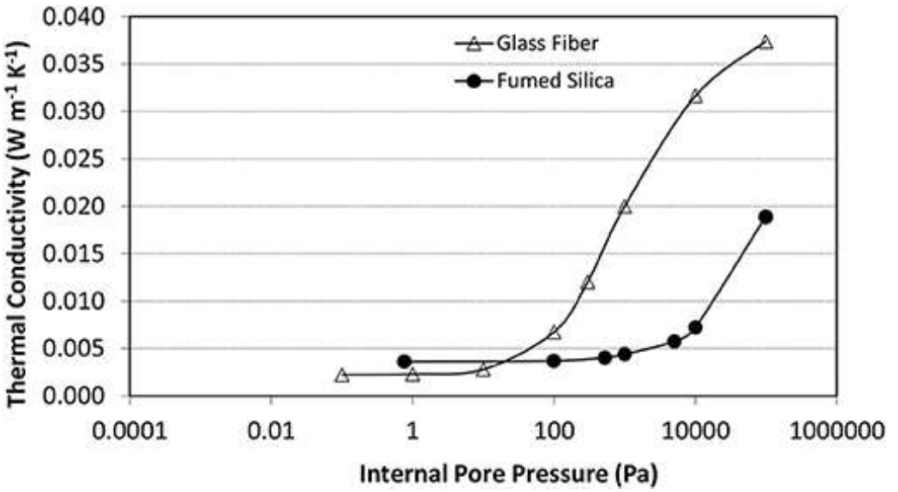

Figure 22: Typical thermal conductivity of glass fiber and fumed silica VIPs as a function of internal pore gas (air) pressure [59].

After 'heat & vapour' aging test, the thermal conductivity of fumed silica VIP specimens (except failed specimen FS8) increased to around 0.007 W/(m·K) (Figure 14) and the thermal conductivity of fiberglass VIP specimens increased to around 0.035 W/(m·K) (Figure 17). Based on the trendlines in Figure 22, fiberglass VIP specimens had relatively higher inner pressure than fumed silica VIP specimens after 'heat & vapour' aging test.

4.2 Results from Vibration Tests

This section presents the recorded data during the random vibration test for six (6) unaged VIP specimens (Fumed silica: FS10, FS11 and FS12; Fiberglass: FG10, FG11 and FG12) in sub-section 4.2.1, and six (6) aged VIP specimens (Fumed silica: FS4, FS6 and FS7; Fiberglass: FG4, FG5 and FG8) in sub-section 4.2.2.

4.2.1 Unaged specimens

The recorded thermal conductivity data of the unaged fumed silica VIP specimens (FS10, FS11 and FS12) subjected to 480 hours of random vibration tests are shown in Figures 23 and 24 below. The percentage change is calculated from dividing the difference between specimen's thermal conductivity measurement and its initial value by its initial value. Sudden increase in thermal conductivity after 240 hours of simulated random vibration test was observed in fumed silica VIP specimen vibrated with load (FS12). Based on the relationship between thermal conductivity and pore pressure (See Figure 22), the increased thermal conductivity value (0.0208 W/m·K) indicated a total vacuum failure. However, the constrained fumed silica VIP specimen subjected to random vibration (FS10) and freely vibrated fumed silica VIP specimen (FS11) did not show any measurable change in thermal conductivity (i.e. no vacuum failure). Hence, based on limited test data, it can be concluded that there exists risk of vacuum failure for fumed silica VIP specimens vibrated with load.

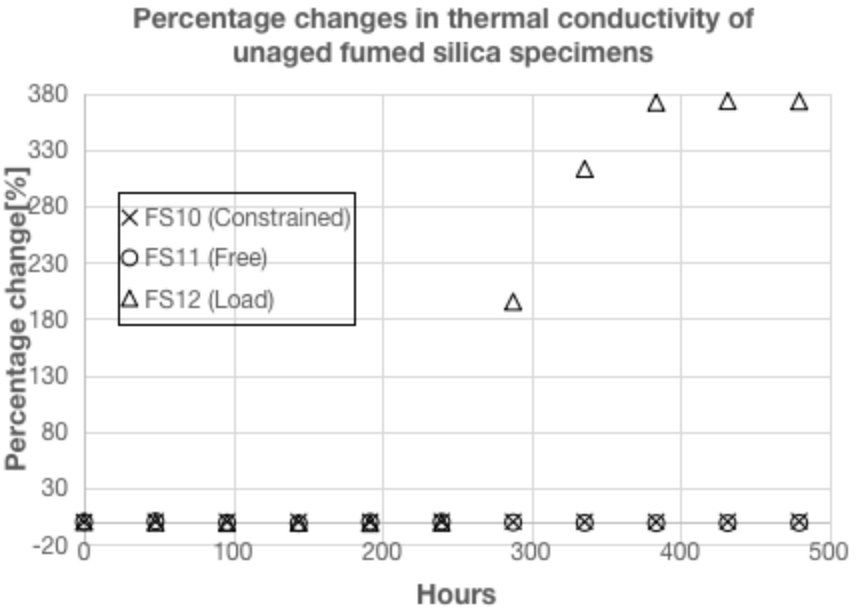

Figure 23: Plot of percentage changes in thermal conductivity of unaged fumed silica specimens in the vibration test.

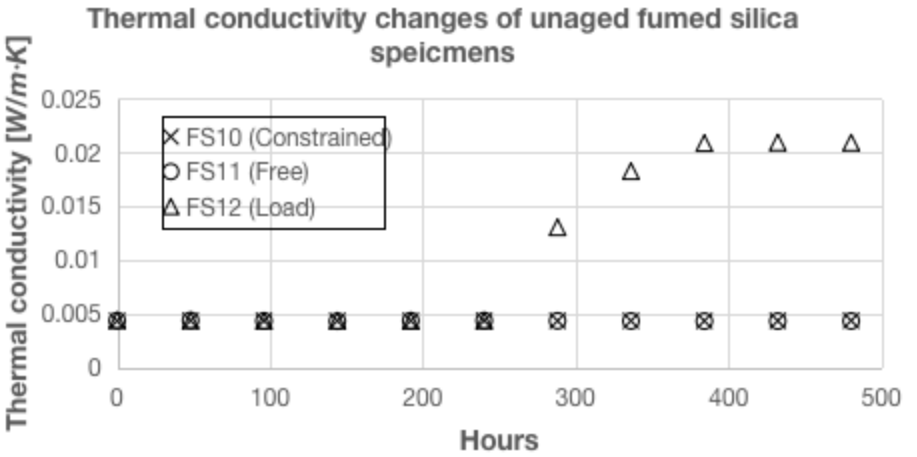

Figure 24: Plot of Thermal conductivity changes of unaged fumed silica specimens.

The recorded thermal conductivity data of the unaged fiberglass VIP specimens (FG10, FG11 and FG12) subjected to 480 hours of random vibration test shown in the Figures 25 and 26 below. The percentage change is calculated from dividing the difference between specimen's thermal conductivity measurement and its initial value by its initial value.

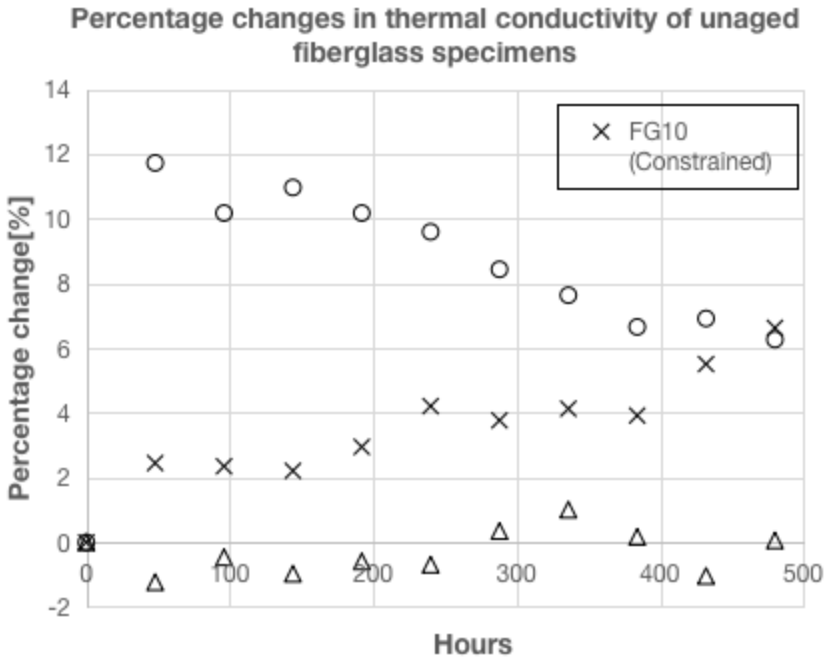

Figure 25: Plot of percentage changes in thermal conductivity of unaged fiberglass specimens in the random vibration test.

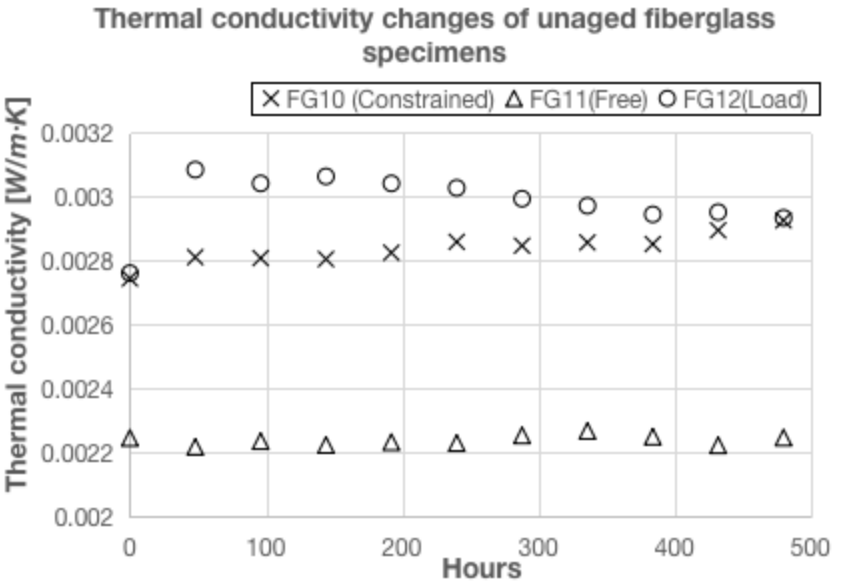

Figure 26: Plot of thermal conductivity changes of unaged fiberglass specimens.

In Figure 26 above, constrained fiberglass VIP specimen subjected to random vibration (FG10) and the freely vibrated fiberglass VIP specimen (FG11) experienced random vibration on their vertical orientation. The supporting clamps tightly constrained fiberglass VIP specimen FG10 on the shaking table, but two soft foam layers sandwiched fiberglass VIP specimen FG11. The accelerometer recorded the acceleration RMS value of fiberglass VIP specimen FG11 as only half of the registered value for fiberglass VIP specimen FG10. A reasonable explanation is that two soft foam layer acts as dampers in this system since their surface friction drags the specimen in the opposite direction when fiberglass VIP specimen FG11 vibrates. That indicates a well-designed damper layer, in the sandwich form with fiberglass VIP specimens, can reduce the vibration level of fiberglass VIP experienced and slow fiberglass VIP performance drop due to vibration. The high-order polynomial trendline describes the aging pattern of specimen FS10,

shown in Figure 27 below. The derived aging pattern for the constrained fiberglass VIP specimen FG10 during the random vibration in Figure 27. The linear best-fit trendline intend to eliminate the errors from apparatus accuracy and random errors.

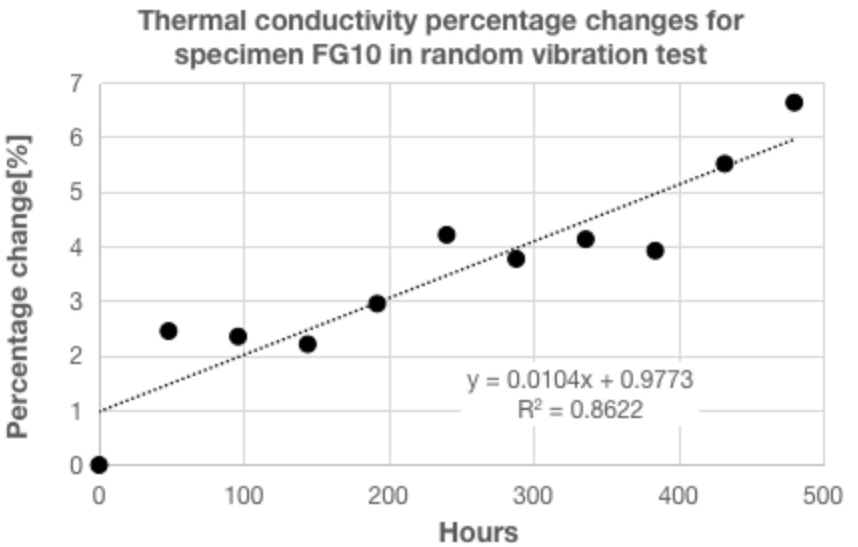

Figure 27: Plot of thermal conductivity percentage changes for specimen FG10 with trendline in the random vibration test.

The recorded data of the vibrated with load fiberglass VIP specimen (FG12) shows a different pattern from the vibrated with load fumed silica VIP specimen (FS12) under the same vibration test condition, where it had an immediate jump after the first test cycle. Then it gradually dropped to round 6%. That indicates fiberglass VIPs are more elastic than fumed silica VIPs and can handle a small amount of load for an extended period instead of a sudden failure. Figures 28 and 29 consist of the plots of both fumed silica VIP specimens (FS10, FS11 and FS12) plotted

according to left vertical axis and fiberglass VIP specimens (FG10, FG11 and FG12) plotted according to right vertical axis for easy comparison.

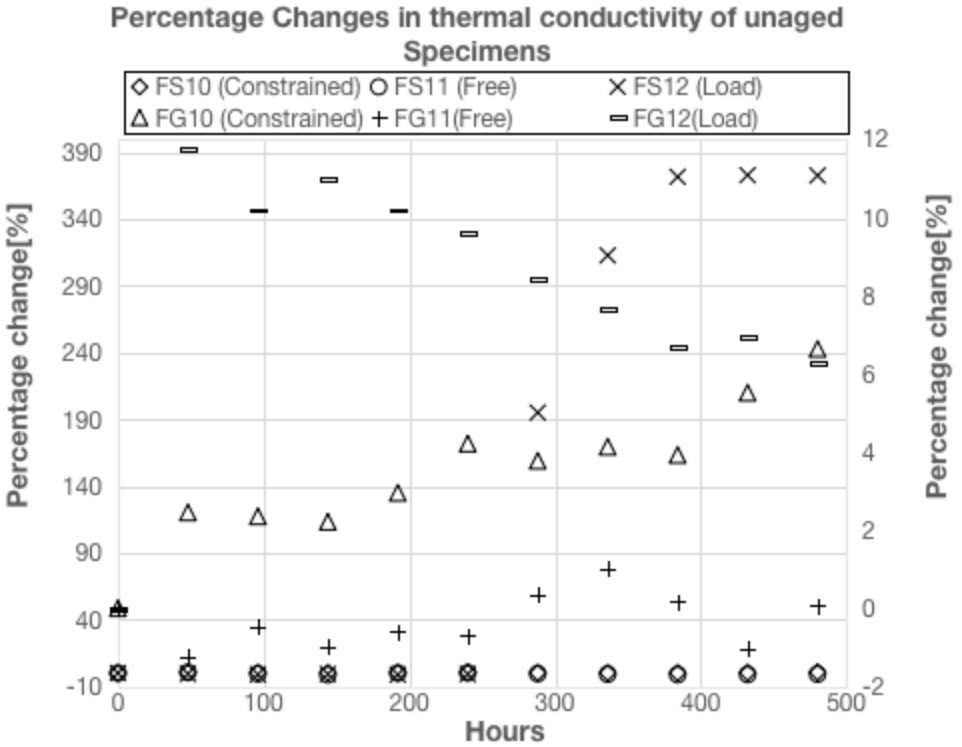

Figure 28: Plots of percentage changes in thermal conductivity of all unaged specimens.

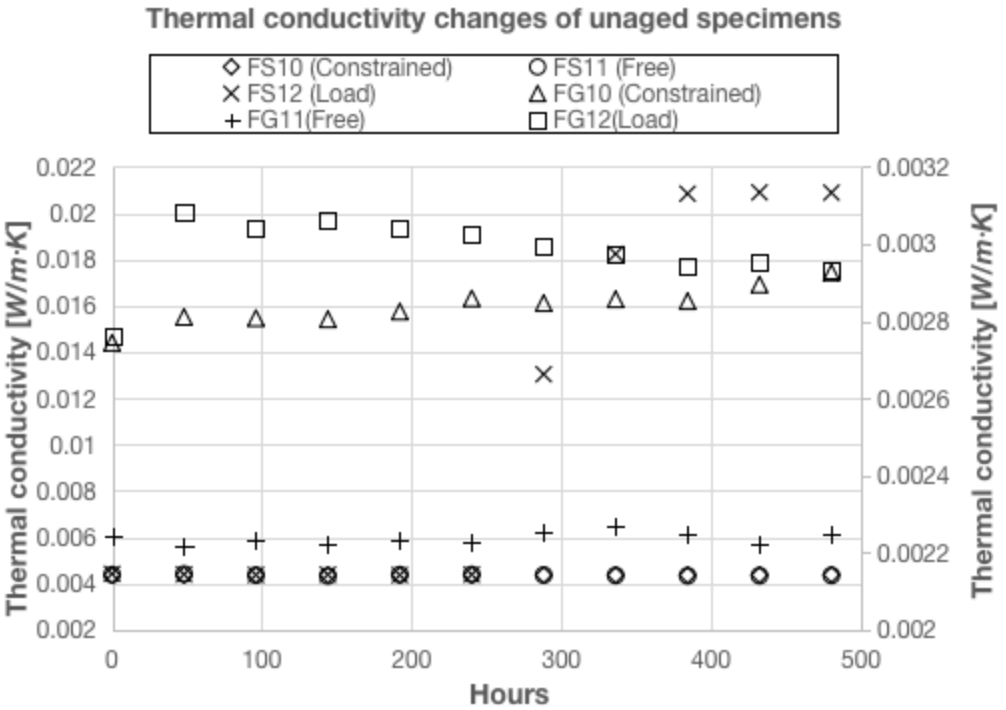

Figure 29: Plot of thermal conductivity changes of all unaged specimens.

To study the fatigue mechanism of VIP in the random vibration test, the mass increases of a VIP specimen are evidence of the envelope or barrier layer broken because the moisture in penetrated air is absorbed by core material and accumulated inside the VIP specimen. In the case of the vibrated with load fumed silica VIP specimen (FS12), its weight started increasing after 240 hours of simulated random vibration test and had a total increase of 2.76 grams. Therefore, there is a high possibility of its vacuum loss results in a sudden degradation of its thermal insulation performance. However, the results of the constrained fiberglass VIP specimen (FG10) and the vibrated with load fiberglass VIP specimen (FG12) did not share the same behavior with fumed

silica VIP specimen FS12 because the weights of fiberglass VIP specimens (both FG10 and FG12) had no noticeable changes after 480 hours of simulated random vibration test. The hypothesis of fiberglass VIP specimen FG10 and FG12 degradation mechanism should relate to another aspect. EBC Annex 65 subtask 1 [60] discussed a unique mechanism named "creep" for VIP mechanically loaded, which is a reasonable answer to the change of specimen FG10 and FG12. The fibers or granularity of core material are rearranged, under the excitation of random vibration, which results in an increase in core density and then leads to an increase in solid conduction. Furthermore, recalling the result of fumed silica VIP specimen vibrated with load (FS12), the fiberglass core shows a more muscular performance to handle loaded vibration in horizontal orientation.

One more thermal conductivity measurement was performed on fiberglass VIP specimen FG12 after 20 days of vibration test completion, and the measurement (8%) showed a slight increase compared with the last measurement (5.8%). This change indicates that the loaded horizontal vibration test has effect on the airtight of fiberglass VIP specimen (FG12), and the inner pressure of this fiberglass VIP specimen increasing slowly after the random vibration test with load. Furthermore, more measurements were also performed on fiberglass VIP specimen FG10 after vibration test completion, and the measurements indicate its thermal conductivity kept increasing even without the excitation of vertical vibration (12.8% at 1-month after vibration test, 16.2% at 2-months after vibration test, and 18.4% at 2.5-months after vibration test). Hence, vacuum loss and fiber rearrangement simultaneously occurred in the case of fiberglass VIP specimen FG10. Recalling the results of fiberglass VIP specimen FG10 and FG12, random vibration on fiberglass VIP has a risk of resulting panel's vacuum loss. More post-test thermal conductivity

measurements were also performed on fumed silica VIP specimens (FS10, FS11, and FG12) after the vibration test completion, but no measurable changes were observed.

4.2.2 Aged specimens

Four (4) aged VIP specimens (Fumed silica: FS6 and FS7; Fiberglass: FG4, and FG8) underwent random vibration test in vertical orientation. Aged fumed silica VIP specimen FS4 and aged fiberglass VIP specimen FG5 underwent random vibration in horizontal orientation with load. Compared with the other aged VIP specimens for both fumed silica and fiberglass core material, those six VIP specimens has relatively minor thermal conductivity increasements after the 'heat' and 'heat & vapour' aging test.

Figure 30 shows the data recorded for aged fiberglass VIP specimen (FG4 from 'heat' aging) after 120 hours of simulated random vibration test, and its thermal conductivity increased by 20% at the end. Recalling Figure 26, the thermal conductivity of unaged fiberglass VIP specimen FG10 increased by 3% at 200 hours of simulated random vibration. That indicates 'heat' aging accelerated fiberglass VIP degradation when subjected to the simulated random vibration test.

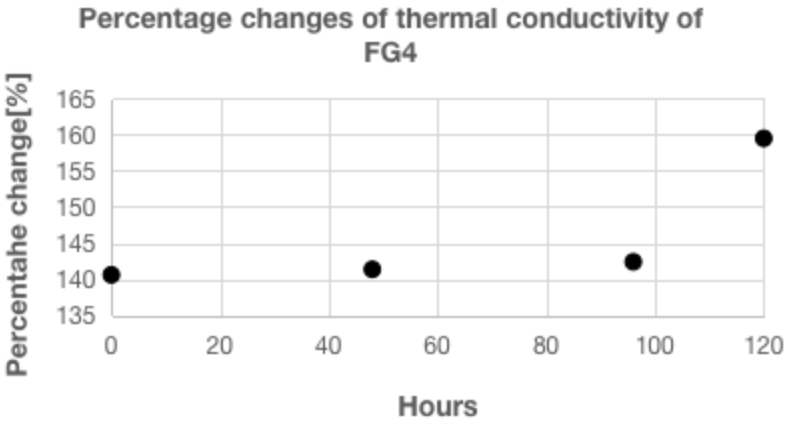

Figure 30: Plot of percentage change of thermal conductivity of specimen FG4.

Figure 31 shows the plot of aged fiberglass VIP specimen (FG8 from 'heat & vapour' aging) subjected to 120 hours of simulated random vibration test, and its thermal conductivity increased by 40% after the test. The aging rate of aged fiberglass VIP specimen FG8 during the random vibration test is about 0.33% per hour vibration, dramatically more remarkable than that of aged fiberglass VIP specimen FG4 (0.02% per hour random vibration). The offset point (at 96 hours) may be caused by the fluctuation of moisture due to unexpected weather change. Since this specimen (FG8) already lost it vacuum in the previous aging test, there is a possibility moisture flow happens easily between the specimen and environment. The accumulated moisture inside fiberglass VIP specimen FG8 is a fatal factor resulting in a faster aging rate, and the moisture worsens the rate of fiberglass VIP vacuum loss.

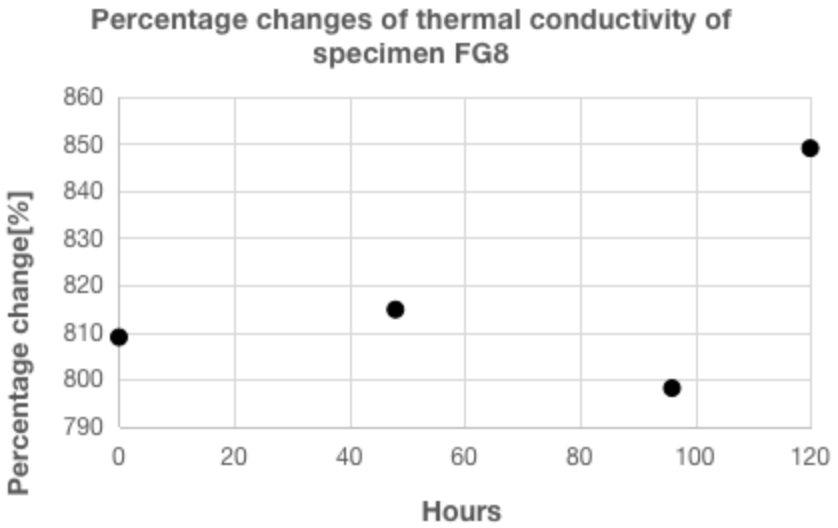

Figure 31: Plot of percentage change of thermal conductivity of specimen FG8.

From Figure 32, the weight of aged fiberglass VIP specimen FG8 was constantly decreasing during 120 hours of simulated random vibration test which represents the constant moisture escape from the fiberglass VIP specimen envelop to the ambient environment. This moisture escape indicates that the above aging rate of fiberglass VIP specimen FG8 (0.33% per hour random vibration) is underestimated for the actual situation because the random vibration test was operated at the laboratory condition (22±1 ° C, 45±5% RH). The aged fiberglass VIP specimen (FG8 from 'heat & vapour' aging test) has higher relative humidity inside its envelope. Hence, during the random vibration test, the moisture inside this fiberglass VIP specimen flowed from high relative humidity area to low relative humidity area.

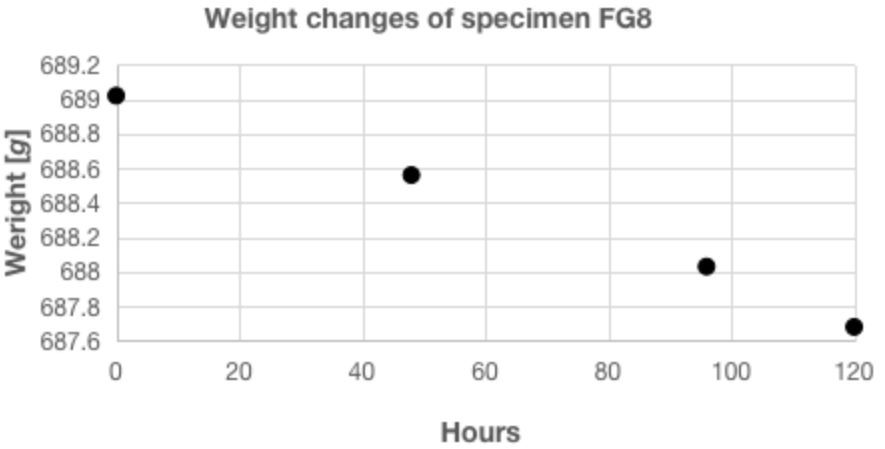

Figure 32: Plot of weight changes of specimen FG8.

Figures 33 and 34 show the results of fumed silica VIP specimens (FS6 from 'heat' aging and FS7 from 'heat & vapour' aging) respectively, subjected to 120 hours of simulated random vibration test at their vertical orientation.

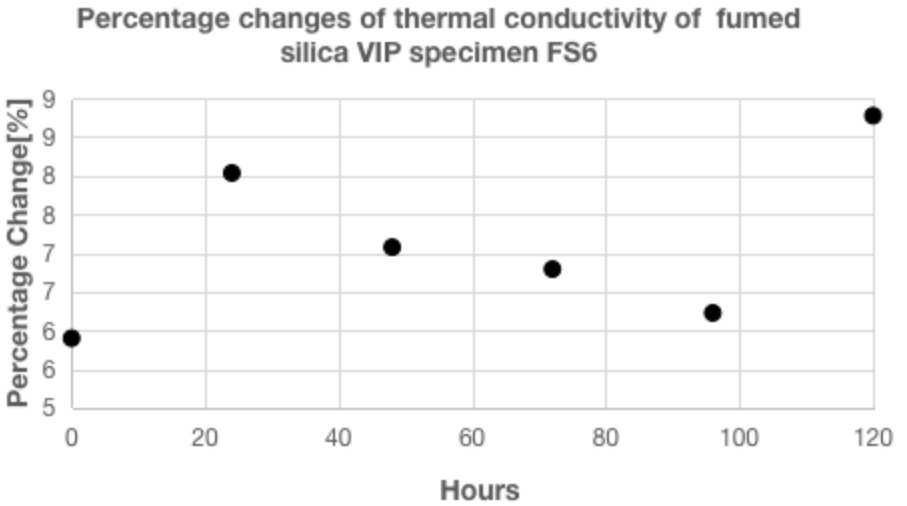

Figure 33: Plot of percentage changes of thermal conductivity of fumed silica VIP specimen FS6.

Figure 33 shows the thermal conductivity increasing rate of fumed silica VIP specimen FS6 was about 0.023% per hour random vibration at the vertical orientation, and the total difference was about 3% after 120-hours random vibration test. The used test apparatus (heat-flow-meter) has 3% accuracy and has a possibility to result some offsets in data above (FS6 in Figure 33). In contrast, in Figure 34, the thermal conductivity increasing rate of fumed silica VIP specimen FS7 was about 0.132% per hour random vibration subjected to the same test, and a total difference was larger than 10% after the same duration random vibration test.

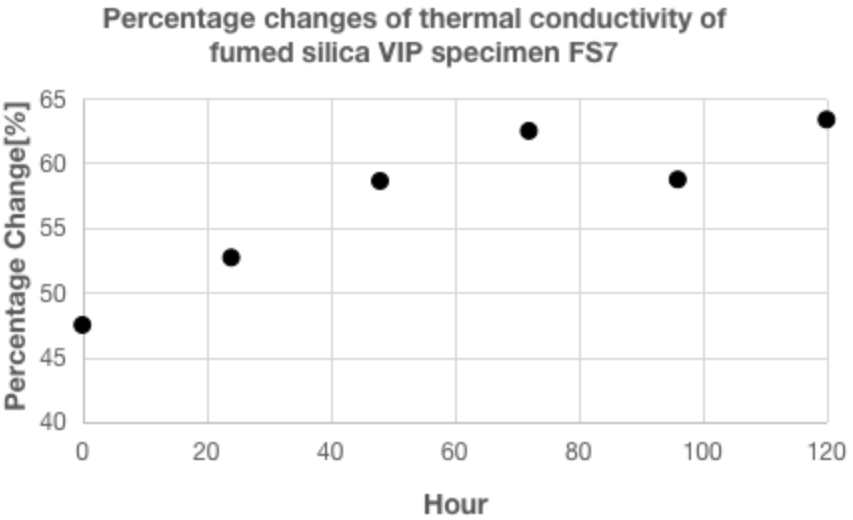

Figure 34: Plot of percentage changes of thermal conductivity of fumed silica VIP specimen FS7.

Figure 35 provides the convenience to compare the aged fumed silica VIP specimen (FS6) (in Figure 33) and the aged fiberglass VIP specimen (FG4) (in Figure 30). Both fumed silica VIP specimen FS6 and fiberglass VIP specimen FG4 underwent the 'heat' aging test before the random vibration test. However, the thermal conductivity of aged fiberglass VIP specimen (FG4) increased by 0.00042 W/m·K while the thermal conductivity of aged fumed silica specimen (FS6) increased by 0.00013 W/m·K. It can conclude that 'heat' aged fiberglass VIP specimen generally has a more significant aging rate (0.0035 m·W/m·K per hour random vibration) than that 'heat' aged fumed silica VIP specimen (0.0011 m·W/m·K per hour random vibration).

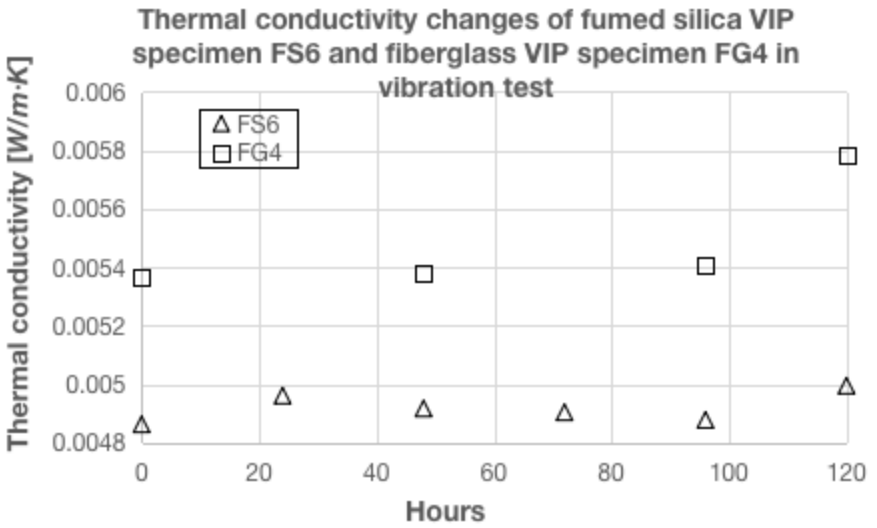

Figure 35: Thermal conductivity changes of fumed silica VIP specimen FS6 and fiberglass VIP specimen FG4 in vibration test.

Figure 36 provides the convenience to compare aged fumed silica VIP specimen (FS7) and aged fiberglass VIP specimen (FG8) both from 'heat & vapour' aging test. The thermal conductivity of aged fumed silica VIP specimen FS7 increased by 0.000689 W/m·K after 120 hours random vibration test, while the thermal conductivity of aged fiberglass VIP specimen FG8 increased by 0.000861 W/m·K after the same test. It can conclude that 'heat & vapour' aged fiberglass VIP has a higher aging rate (0.007175 m·W/m·K per hour random vibration) than 'heat & vapour' aged fumed silica VIP specimen (0.005742 m·W/m·K per hour random vibration). Hence, fumed silica VIP specimen FS7 produced a slow change in its thermal conductivity comparing with fiberglass VIP specimen FG8. Recalling the results of 'heat' aged VIP specimens, both 'heat' and 'heat & vapour' aged fumed silica VIPs had lower aging rate than that of fiberglass VIPs.

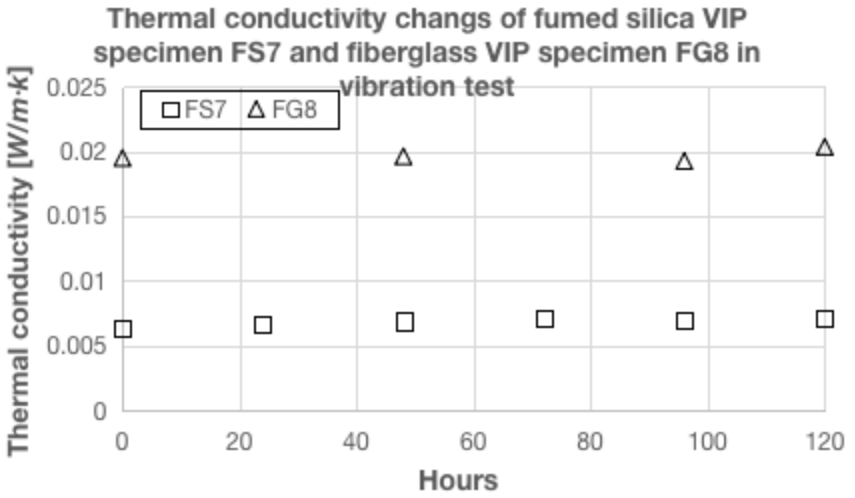

Figure 36: Thermal conductivity changes of fumed silica VIP specimen FS7 and fiberglass VIP specimen FG8 in vibration test.

The recorded data of fiberglass VIP specimen (FG5) subjected to 120 hours of simulated random vibration test at their horizontal orientations with 14kPa load are shown in Figures 37 below. Figure 37 shows that the thermal conductivity of fiberglass VIP specimen FG5 increased by about 12% after 120 hours of simulated random vibration.

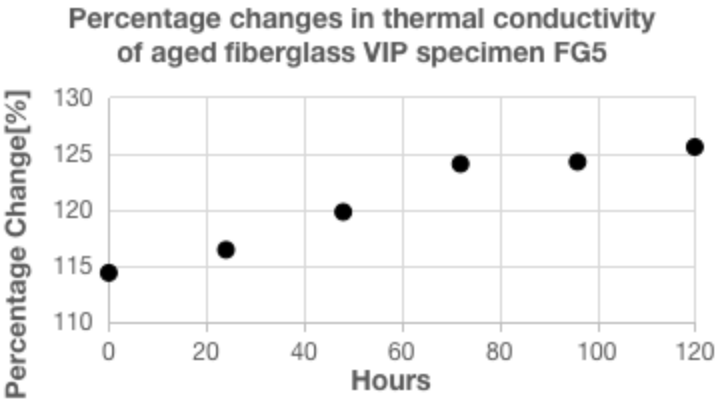

Figure 37: Plot of Percentage changes in thermal conductivity of aged fiberglass VIP specimen FG5.

In order to compare the change in thermal conductivity between aged and unaged fiberglass VIP specimen (FG5 and FG12), the first 144-hour data points of unaged fiberglass VIP specimen FG12 (in Figure 25) are used to create Figure 38 below. In Figure 38, the data of fiberglass VIP specimen FG12 was plotted according to left vertical axis, while the data of fiberglass VIP specimen FG5 was plotted according to right vertical axis. The changes in thermal conductivity of 'heat' aged fiberglass VIP specimen FG5 and unaged fiberglass VIP specimen FG12 in Figure 38 proposes that fiberglass VIP has a high possibility of thermal conductivity increase when subjected to a constant random vibration with loads applied on its surface. Aged fiberglass VIP (with more moisture accumulated inside the envelope) degraded faster.

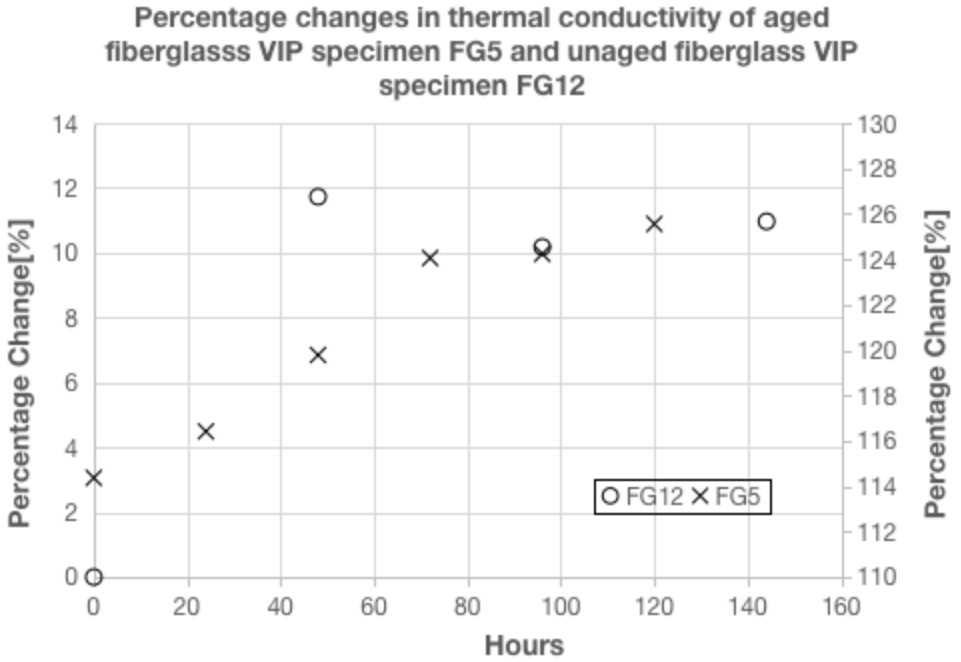

Figure 38: Plot of Percentage changes in thermal conductivity of aged fiberglass VIP specimen FG5 and unaged fiberglass VIP specimen FG12.

Recalling the result in Figure 30, the thermal conductivity of 'heat' aged fiberglass VIP specimen FG4 increased by about 20% after 120 hours of simulated random vibration at its vertical orientation. Fiberglass VIP specimen FG4 and FG5 experienced the same 'heat' aging test. However, fiberglass VIP specimen FG4 (constrained, vertical) had larger change in its thermal conductivity after vibration test comparing with fiberglass VIP specimen FG5 (vibrated with load, horizontal). That indicates random vibration along fiberglass VIP's vertical orientation will result in a more considerable performance drop.

Figure 39 below shows the thermal conductivity changes of aged fumed silica VIP specimen FS4 ('heat' aging) after 120 hours of simulated random vibration with 14kPa load at its horizontal orientation. The maximum absolute deviation of this data set was 0.44%, which is in the range of the heat-flow-meter's accuracy (3%). Hence the thermal conductivity of specimen FS4 is assumed to be unchanged after this simulated random vibration test.

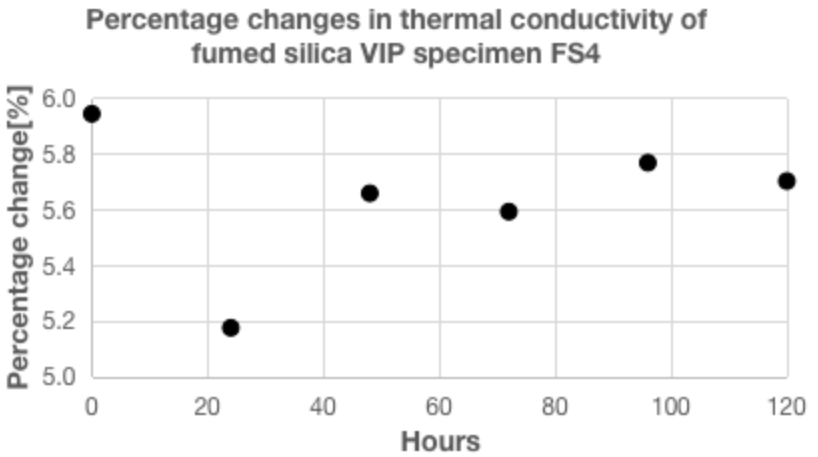

Figure 39: Plot of Percentage changes in thermal conductivity of fumed silica VIP specimen FS4.

Figure 40 below compares the results of 'heat' aged fumed silica VIP specimen (FS4) and 'heat' aged fiberglass VIP specimen (FG5) subjected to random vibration with 14kPa load, which shows the percentage changes of thermal conductivity respecting to their values at the beginning of vibration test. The aged fiberglass VIP specimen (FG5) had a larger thermal conductivity increasement (5%) than the aged fumed silica VIP specimen (FS4), after 120 hours vibration test.

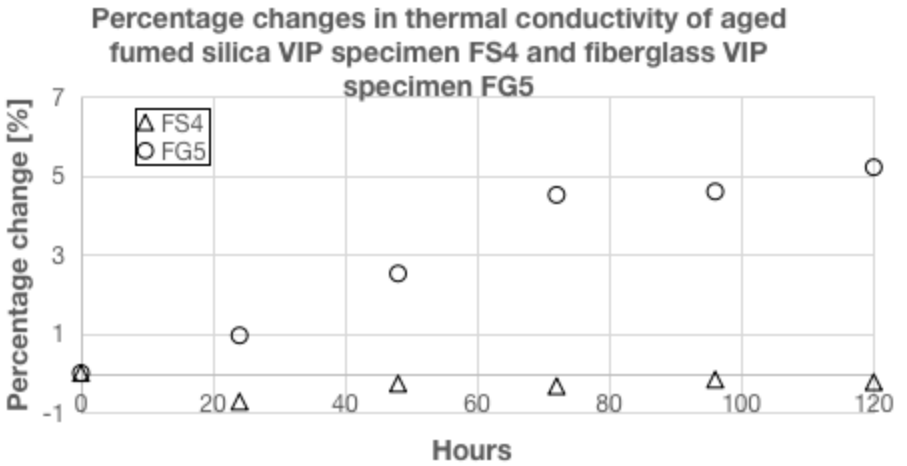

Figure 40: Plot of Percentage changes in thermal conductivity of aged fumed silica VIP specimen FS4 and fiberglass VIP specimen FG5.

Figure 41 shows a plot that summarizes the results of all aged VIP specimens (fumed silica and fiberglass), representing the difference in percentages between the thermal conductivity of each VIP specimen at the beginning and the end of the simulated random vibration test. The data of fumed silica VIP specimens were plotted according to left vertical axis, while the data of fiberglass VIP specimens were plotted according to right vertical axis. The percentage change is calculated from dividing the difference between specimen's thermal conductivity measurement and its starting value at the beginning of vibration test by its starting value. This difference is attributed to each aged VIP specimen's different initial thermal conductivity. Figure 41 demonstrates the aged fumed silica VIP specimen had a lower average degradation rate than that of aged fiberglass VIP specimen subjected to 120 hours vibration test. Furthermore, by comparing the worst scenario, the thermal conductivity of fiberglass VIP increased 40.2% after the simulated vibration test while that of fumed silica VIP increased 15.9% after the same test.

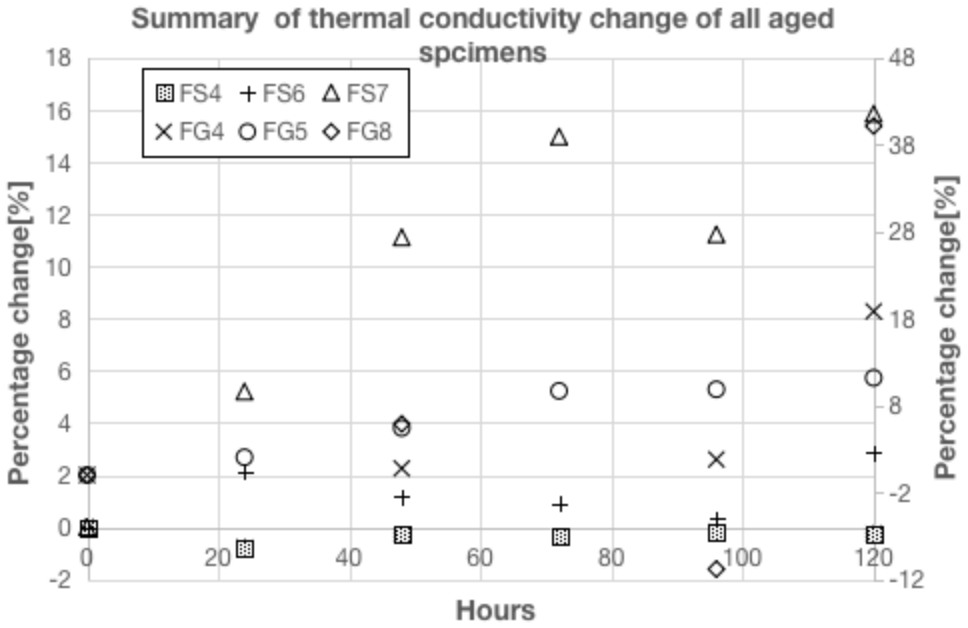

Figure 41: Plot of summary of thermal conductivity change of all aged specimens subjected to the simulated random vibration test.

5. Conclusions

- This paper investigated the impact of random vibration on the performance of vacuum insulation panels (VIPs) used in the construction of energy-efficient shipping containers. Both aged (heat aging: 70±1 °C, 5±3% RH up to 120 days; heat and vapour aging: 70±1 °C, 95±3% RH up to 120 days) and unaged (laboratory, 22±1 °C, 45±5% RH) fumed silica and fiberglass core VIP specimens (300 mm x 300 mm x 25 mm) were subjected to random vibration tests, following ASTM standards D4169 and D4728, representing in service truck vibration, under various loading and constraint conditions. The thermal conductivity and mass of the specimens were measured at regular intervals. Overall, experimental observations indicate that truck vibrations could impact the long-term thermal characteristics of Vacuum Insulation Panels (VIPs). However, this impact is more evident in fibreglass core VIPs than in fumed silica core VIPs. More specific findings from this study are outlined below.

- In both 'heat' and 'heat & vapour' aging, fiberglass core specimens aged faster than fumed silica core specimens. While the thermal conductivity of aged fumed silica VIP specimens changed up 0.007 W/(m·K) but the same for the fiberglass VIP specimens was up to 0.035 W/(m·K).
- 60 days for fiberglass VIP specimens in 'heat & vapour' aging test is a critical point. After this point, fiberglass VIP specimens lost it vacuum in a short period of time.
- Unaged fumed silica VIP specimens can handle the lower in-service truck random vibration in vertical orientation without noticeable thermal conductivity increase. However, a failure was observed after 240 hours vibration when unaged fumed silica VIP vibrated with 14kPa load on its horizontal orientation.

- Simulated random vibration resulted to unexpected thermal conductivity increases in unaged fiberglass VIP specimens.

The limitations of this study are:

1. The aged specimens from the water vapor aging test contain moisture inside the envelope, and the bi-directional moisture flow is activated by replacing them at ambient conditions for the random vibration test. Thus, the bi-directional moisture flow could cause errors in measuring the specimen's thermal conductivity.
2. The used acceleration RMS level of truck random vibration is the lower limit of truck in-service data, although interesting changes in the specimen's performance have been observed.
3. The load applied to horizontal-orientated specimens is not uniform across their top surface due to the capability shortage of our shaker, and the non-uniform distributed load cannot always represent the working conditions of a shipping container.
4. Due to the time limitation, 12 VIP specimens experienced random vibration tests, and the test duration is up to 480 hours. Need to test more VIPs for longer time.
5. The unexpected weather fluctuation could contribute to some offset during the test.
6. The envelop or barrier design of fumed silica VIP specimens and fiberglass VIP specimens are different. The information about getters/desiccants inside the VIP envelop is restricted by the VIP manufacturers, and those components may also contribute to some errors in this research.

6. Future Works

Future work is required to examine the repeatability and diversity (size, origin etc.) of test results. High acceleration RMS or shock vibration test should be planned for some rare scenarios during transportation, such as collision. A high vibration level has a higher possibility of VIPs' sudden performance failure. Besides that, this study included the typical truck PSD profile, but the insulated shipping container can also be applied to aircraft, vessels, or even rockets. Although vibration will be robust and complicated when fluid motion is involved, it is worth testing VIP with various PSD profiles. The simulated random vibration test performed in this research assumed a simple assembly of VIPs in a shipping container. However, the different assemblies of insulating walls will result in different structural responses, which is an essential factor in investigating vibration responses. The ideal solution is to vibrate a VIP-integrated shipping container, scaling down to the capability of the shaker and the testing. For aged specimens, especially post-test specimens from the 'heat & vapour' aging, reconditioning time is required for moisture diffusion, and one day is not sufficient for reducing the effect of free moisture inside the VIP. In the future, researcher can consider perform the aging test and simulated random vibration test at the same time on VIPs. When testing different core material VIPs, the barrier, getters, and desiccants should keep consistence in all the specimens to avoid uncertainty due to their different envelope or barrier design. Furthermore, the SEM image of VIP specimens after vibration is helpful to verify the orientation of fiber or silica powder due to the induced vibration.

Reference

[1] Cold Chain Market Size Worth $628.26 Billion By 2028 | CAGR: 14.8%: Grand View Research, Inc. (2021, April 29). PR Newswire, NA. https://link.gale.com/apps/doc/A659998730/ITBC?u=uvictoria&sid=bookmark-ITBC&xid=5930a1a3

[2] “12.3.1 Global Food losses : www.fao.org,” 12.3.1 Global food losses | Sustainable Development Goals | Food and Agriculture Organization of the United Nations,

[3] H. Li and P. Pan, “Food Waste in Developed Countries and Cold Chain Logistics,” in E3S Web of Conferences, 2021, vol. 251, p. 3001–. doi: 10.1051/e3sconf/202125103001.

[4] B. Marchi and S. Zanoni, “Cold Chain Energy Analysis for Sustainable Food and Beverage Supply,” Sustainability (Basel, Switzerland), vol. 14, no. 18, p. 11137–, 2022, doi: 10.3390/su141811137.

[5] Dai, J., Che, W., Lim, J. J., & Shou, Y. (2020). Service innovation of cold chain logistics service providers: A multiple-case study in China. Industrial Marketing Management, 89, 143–156. https://doi.org/10.1016/j.indmarman.2019.08.002

[6] Carson, J. K., & East, A. R. (2018). The cold chain in New Zealand – A review. International Journal of Refrigeration, 87, 185–192. https://doi.org/10.1016/j.ijrefrig.2017.09.019

[7] India Cold Chain Logistics Market Report 2022: Featuring Key Players Snowman Logistics, Gati Kausar, ColdEx Logistics & Others - ResearchAndMarkets.com. (2022, July 30). Investment Weekly News, 230. https://link.gale.com/apps/doc/A711304520/ITBC?u=uvictoria&sid=bookmark-ITBC&xid=d828d5a2

[8] Ikegaya, A., Ohba, S., Nakajima, T., Toyoizumi, T., Ito, S., & Arai, E. (2020). Practical long‐term storage of strawberries in refrigerated containers at ice temperature. Food Science & Nutrition, 8(9), 5138–5148. https://doi.org/10.1002/fsn3.1817

[9] Arduino, G., Carrillo Murillo, D., & Parola, F. (2015). Refrigerated container versus bulk: evidence from the banana cold chain. Maritime Policy and Management, 42(3), 228–245. https://doi.org/10.1080/03088839.2013.851421

[10] Frank, K. (1999). Monitoring temperature-sensitive vaccines and immunologic drugs, including anthrax vaccine. American Journal of Health-System Pharmacy, 56(20), 2052–2055. https://doi.org/10.1093/ajhp/56.20.2052

[11] Macklin, G. (2004). RCS builds custom containers for chemical shipments. Refrigerated Transporter, 39(33), 20–.

[12] Green Cooling Initiative. (2022). Global greenhouse gas emissions from the RAC sector.

[13] Dong, Y., & Miller, S. A. (2021). Assessing the lifecycle greenhouse gas (GHG) emissions of perishable food products delivered by the cold chain in China. Journal of Cleaner Production, 303, 126982–. https://doi.org/10.1016/j.jclepro.2021.126982

[14] Wu, W., Beretta, C., Cronje, P., Hellweg, S., & Defraeye, T. (2019). Environmental trade-offs in fresh-fruit cold chains by combining virtual cold chains with life cycle assessment. Applied Energy, 254, 113586–. https://doi.org/10.1016/j.apenergy.2019.113586

[15] Filina-Dawidowicz, L., Filin, S., Wojnicz, L., Miłek, D., & Grzelak, P. (2022). Energy-efficient maritime transport of refrigerated containers. *Procedia Computer Science*, *207*, 3572–3581. https://doi.org/10.1016/j.procs.2022.09.416

[16] Getahun, S., Ambaw, A., Delele, M., Meyer, C. J., & Opara, U. L. (2017). Analysis of airflow and heat transfer inside fruit packed refrigerated shipping container: Part I – Model development and validation. Journal of Food Engineering, 203, 58–68. https://doi.org/10.1016/j.jfoodeng.2017.02.010

[17] Zhao, X., Huang, Y., Chen, J., Su, P., Sha, F., & Yuan, Y. (2021). Numerical simulation of air flow and heat transfer in air refrigerated containers using clean energy technologies. IOP Conference Series. Earth and Environmental Science, 804(4), 42068–. https://doi.org/10.1088/1755-1315/804/4/042068

[18] Kayansayan, N., Alptekin, E., & Ezan, M. A. (2017). Thermal analysis of airflow inside a refrigerated container. International Journal of Refrigeration, 84, 76–91. https://doi.org/10.1016/j.ijrefrig.2017.08.008

[19] Senguttuvan, S., Youn, J.-S., Park, J., Lee, J., & Kim, S.-M. (2020). Enhanced airflow in a refrigerated container by improving the refrigeration unit design. International Journal of Refrigeration, 120, 460–473. https://doi.org/10.1016/j.ijrefrig.2020.08.019

[20] Helion fuel cells to power refrigerated maritime containers. (2020). Fuel Cells Bulletin, 2020(8), 6–6. https://doi.org/10.1016/S1464-2859(20)30339-4

[21] Alzuwaid, F. A., Ge, Y. T., Tassou, S. A., & Sun, J. (2016). The novel use of phase change materials in an open type refrigerated display cabinet: A theoretical investigation. Applied Energy, 180, 76–85. https://doi.org/10.1016/j.apenergy.2016.07.088

[22] Mousazade, A., Rafee, R., & Valipour, M. S. (2020). Thermal performance of cold panels with phase change materials in a refrigerated truck. International Journal of Refrigeration, 120, 119–126. https://doi.org/10.1016/j.ijrefrig.2020.09.003

[23] Fioretti, R., Principi, P., & Copertaro, B. (2016). A refrigerated container envelope with a PCM (Phase Change Material) layer: Experimental and theoretical investigation in a representative town in Central Italy. Energy Conversion and Management, 122, 131–141. https://doi.org/10.1016/j.enconman.2016.05.071

[24] Copertaro, B., Principi, P., & Fioretti, R. (2016). Thermal performance analysis of PCM in refrigerated container envelopes in the Italian context – Numerical modeling and validation. Applied Thermal Engineering, 102, 873–881. https://doi.org/10.1016/j.applthermaleng.2016.04.050

[25] Wang, J., Ma, X., Sun, Y., & Xie, J. (2023). Thermal performance and sustainability assessment of refrigerated container with vacuum insulation panel envelope layer at different design forms. Thermal Science and Engineering Progress, 42. https://doi.org/10.1016/j.tsep.2023.101928

[26] Hammond, E. C., & Evans, J. A. (2014). Application of Vacuum Insulation Panels in the cold chain – Analysis of viability. International Journal of Refrigeration, 47, 58–65. https://doi.org/10.1016/j.ijrefrig.2014.07.010

[27] Kan, A., Zhu, W., Wang, T., Yuan, Y., & Zhang, X. (2021). Thermal performance assessment of cold chain chamber with vacuum insulation panel envelope layer. Cleaner Engineering and Technology, 4, 100157–. https://doi.org/10.1016/j.clet.2021.100157

[28] Gaedtke, M., Wachter, S., Kunkel, S., Sonnick, S., Rädle, M., Nirschl, H., & Krause, M. J. (2020). Numerical study on the application of vacuum insulation panels and a latent heat storage for refrigerated vehicles with a large Eddy lattice Boltzmann method. Heat and Mass Transfer, 56(4), 1189–1201. https://doi.org/10.1007/s00231-019-02753-4

[29] Jelle, B. P. (2011). Traditional, state-of-the-art and future thermal building insulation materials and solutions – Properties, requirements and possibilities. Energy and Buildings, 43(10), 2549–2563. https://doi.org/10.1016/j.enbuild.2011.05.015

[30] Mukhopadhyaya, P., MacLean, D., Korn, J., van Reenen, D., & Molleti, S. (2014). Building application and thermal performance of vacuum insulation panels (VIPs) in Canadian subarctic climate. Energy and Buildings, 85, 672–680. https://doi.org/10.1016/j.enbuild.2014.08.038

[31] Wernery, J., Brunner, S., Weber, B., Knuth, C., & Koebel, M. M. (2021). Superinsulation Materials for Energy-Efficient Train Envelopes. Applied Sciences, 11(7), 2939–. https://doi.org/10.3390/app11072939

[32] International Electrotechnical Commission. (2010). IEC61373 Railway applications-Rolling stock equipment-Shock and vibration tests.

[33] Kraus, E., Hack, U., Baudrit, B., Heidemeyer, P., Bastian, M., Wollheim, T., Caps, R., Wiegmann, W., & Fricke, M. (2016). Under high dynamic load. *ADHESION ADHESIVES&SEALANTS*, *13*(2), 34–39. https://doi.org/10.1007/s35784-016-0013-6

[34] H. Simmler, S. Brunner, U. Heinemann, H. Schwab, K. Kumaran, P. Mukhopadhyaya, D. Quénard, H. Sallée, K. Noller, E. Kükükpinar-Niarchos, C. Stramm, M. Tenpierik, H. Cauberg, M. Erb, Vacuum Insulation Panels. Study on VIP-components and panels for service life prediction of VIP in building applications (Subtask A), Technical Report, IEA/ECBCS Annex 39 HiPTI-project (High Performance Thermal Insulation for Buildings and Building Systems), 2005.

[35] Mukhopadhyaya, P., Molleti, S., & Reenen, D. van. (2014, August). What is a vacuum insulation - the International Institute of Building ... Vacuum Insulation Panels (VIPs): AN HISTORIC OPPORTUNITY FOR THE BUILDING CONSTRUCTION INDUSTRY. https://iibec.org/wp-content/uploads/2014-08-mukhopadhyaya-molleti-vanreenen.pdf

[36] Guan, X., Shu, N., & Peng, H. (2021). LBM simulation of heat transfer processes inside GIS capsule filled with different insulation gas mixtures. Mathematics and Computers in Simulation, 188, 212–225. https://doi.org/10.1016/j.matcom.2021.03.033

[37] He, Y.-L., & Xie, T. (2015). Advances of thermal conductivity models of nanoscale silica aerogel insulation material. Applied Thermal Engineering, 81, 28–50. https://doi.org/10.1016/j.applthermaleng.2015.02.013

[38] Kalnæs, S. E., & Jelle, B. P. (2014). Vacuum insulation panel products: A state-of-the-art review and future research pathways. Applied Energy, 116, 355–375. https://doi.org/10.1016/j.apenergy.2013.11.032

[39] Kan, A., Zheng, N., Zhu, W., Cao, D., & Wang, W. (2022). Innovation and development of vacuum insulation panels in China: A state-of-the-art review. Journal of Building Engineering, 48, 103937–. https://doi.org/10.1016/j.jobe.2021.103937

[40] SIMMLER, H., & BRUNNER, S. (2005). Vacuum insulation panels for building application Basic properties, aging mechanisms and service life. Energy and Buildings, 37(11), 1122–1131. https://doi.org/10.1016/j.enbuild.2005.06.015

[41] Kim, J.-H., Boafo, F. E., Kim, S.-M., & Kim, J.-T. (2017). Aging performance evaluation of vacuum insulation panel (VIP). Case Studies in Construction Materials, 7(C), 329–335. https://doi.org/10.1016/j.cscm.2017.09.003

[42] Kan, A., Zheng, N., Wu, Y., Wang, W., Zhang, X., Cai, H., & Cao, D. (2022). Theoretical prediction and aging experimental verification of the service life of vacuum insulation panels. Cleaner Engineering and Technology, 8, 100484–. https://doi.org/10.1016/j.clet.2022.100484

[43] Kunič, R. (2012). Vacuum Insulation Panels - An Assessment of the Impact of Accelerated Ageing on Service Life. Strojniški Vestnik – Journal of Mechanical Engineering, 58(10), 598–606. https://doi.org/10.5545/sv-jme.2012.539

[44] Chonhenchob, V., Singh, S. P., Singh, J. J., Sittipod, S., Swasdee, D., & Pratheepthinthong, S. (2010). Measurement and analysis of truck and rail vibration levels in Thailand. Packaging Technology & Science, 23(2), 91–100. https://doi.org/10.1002/pts.881

[45] Zhou, R., Yan, L., Li, B., & Xie, J. (2015). Measurement of Truck Transport Vibration Levels in China as a Function of Road Conditions, Truck Speed and Load Level: Vibration as a Function of Road Conditions, Truck Speed and Load Mass. Packaging Technology & Science, 28(11), 949–957. https://doi.org/10.1002/pts.2176

[46] Garrido, M., Esteban, L., Navarro, P., Herranz, N., Zabaleta, F. J., & Rouillard, V. (2023). Measurement and analysis of truck vibration levels in logistic Spain distribution to simulate package testing. Packaging Technology & Science, 36(7), 585–594. https://doi.org/10.1002/pts.2730

[47] Singh, J., Singh, S. P., & Joneson, E. (2006). Measurement and analysis of US truck vibration for leaf spring and air ride suspensions, and development of tests to simulate these conditions. Packaging Technology & Science, 19(6), 309–323. https://doi.org/10.1002/pts.732

[48] ASTM, D4169-22, Standard Practice for Performance Testing of Shipping Containers and Systems. ASTM International, West Conshohocken, PA (2022) www.astm.org.

[49] ASTM, D4728-17, Standard Test Method for Random Vibration Testing of Shipping Containers. ASTM International, West Conshohocken, PA (2016) www.astm.org.

[50] ISTA, Procedure 3H, Performance Test for Products or Packaged Products in Mechanically Handled Bulk Transport Containers. International Safe Transit Association, East lansing 2009.

[51] ISO 13355, Packaging – Complete, filled transport packages and unit loads – Vertical random vibration test, International Organization for Standardization, 2016.

[52] MIL-STD-810G, Environmental Engineering Consideration and Laboratory tests, Method 514.6. Annex C, Transportation Tailoring Guidance for Vibration Exposure Definition, US Department of Defense, 2008.

[53] Shires, D. (2011). On the time compression (test acceleration) of broadband random vibration tests. Packaging Technology & Science, 24(2), 75–87. https://doi.org/10.1002/pts.915

[54] Palacios, A., Cong, L., Navarro, M. E., Ding, Y., & Barreneche, C. (2019). Thermal conductivity measurement techniques for characterizing thermal energy storage materials – A review. Renewable & Sustainable Energy Reviews, 108, 32–52. https://doi.org/10.1016/j.rser.2019.03.020

[55] ASTM, C518-21, Standard Test Method for Steady-State Thermal Transmission Properties by Means of the Heat-flow-meter Apparatus, ASTM International, West Conshohocken, PA (2021) www.astm.org.

[56] "Vacuum insulated panels: Vacupor insulation," Vacuum Insulated Panels | Vacupor Insulation, https://www.morganthermalceramics.com/en-gb/products-systems/vacuum-insulation-panels-vip/

[57] "ADVANC-R® VIP," Panasonic Industrial Devices, https://na.industrial.panasonic.com/products/building-products/thermal-insulation/lineup/advancr-vip (accessed Mar. 23, 2024).

[58] Wang, Z., & Wang, L. (2017). Accelerated Random Vibration Testing of Transport Packaging System Based on Acceleration PSD. Packaging Technology & Science, 30(10), 621–643. https://doi.org/10.1002/pts.2306

[59] U. Heinemann, etc . (2017). Long-Term Performance of Super-Insulating Materials in Building Components and Systems, Energy in Buildings and Communities Programme.

[60] IEA-EBC Annex 65 research project – VIPA international. (2021, November 24). VIPA International. https://vipa-international.org/iea-ebc-annex65-project/

Appendix I – Fumed Silica VIP Datasheet

Morgan Advanced Materials

POREXTHERM

Data sheet

ENGLISH

VACUPOR® MS

Vacuum-Insulation-Panel (VIP) with double middle seam.

Description

VACUPOR® MS is a microporous insulation material with an extremely low coefficient of thermal conductivity, i.e. with very good insulating properties.

VACUPOR® MS consists basically of inorganic oxides. The main constituent is fumed silica, the other components are opacifiers for minimizing infrared radiation, and silicates.

The barrier film wrapping of VACUPOR® MS isprocessed in form of a double middle seam. This results in a particularly good surface quality. Due to the missing side flaps, the panels can almost be form-fit sticked together butt joint. In foaming processes the foam flow is significantly less constrained, and the formation of cavities is significantly reduced.

VACUPOR® MS (core material) is not flammable and is classified A1 according to DIN ISO EN 13501-1. VACUPOR® MS is heat sealed in a metallized, multilayer plastic film under vacuum. The very low internal pressure and the microporous panel core is responsible for the extremely low thermal conductivity values.

Application

VACUPOR® MS was specifically developed for vacuum insulation applications in the appliance- / refrigeration industry, where increased demands on the surface, dimensional stability, defined formats and foaming properties are defined.

Due to various technical improvements the performance of VACUPOR® MS systems could be reduced significantly.

Typical applications

VACUPOR® MS is also sucessfully used as insulation material in the following areas:

- Refrigerators and freezers
- Cryogenic freezers
- Temperature controlled packaging

Form of delivery

Standard sizes:

1200 mm x 1000 mm
1200 mm x 500 mm
1000 mm x 600 mm
1000 mm x 300 mm
600 mm x 500 mm
600 mm x 250 mm

Standard thicknesses:

10[1], 15, 20, 25, and 30 mm
Further thicknesses on request.

[1] panels of a thickness ≤ 15mm can be supplied without edge folding only.

Customized formats available on request.

Restrictions on applications

The metallized, multilayer plastic film of the VACUPOR® MS must not be damaged by drilling, cutting, milling, nailing or the like, since the interior pressure of the panel will rise and the special properties of the panel, in particular its excellent insulation characteristics, will be lost.

Shelf life

VACUPOR® MS has a very long shelf life. Please also observe our pressure rise table: Thermal conductivity as a function of internal pressure.

Safety directions

VACUPOR® MS is not a hazardous material as defined in EU directive 2006/1907/EEC. Please also observe our material safety data sheet.

VACUPOR® MS does not liberate hazardous decomposition products and, as far as is known at present, does not cause any problems to human health or the environment.

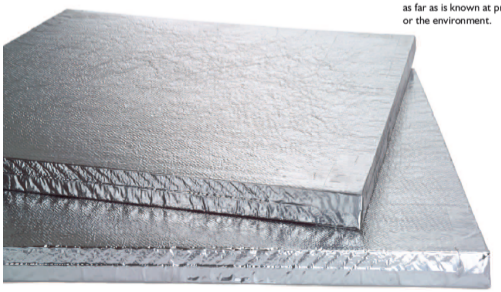

Morgan Advanced Materials

POREXTHERM

Data sheet

VACUPOR® MS

Physical properties (applicable to standard format)		
Colour (Caused by film)		Silver
Density (kg/m³)		160 - 190
Thermal conductivity (W/m·K) DIN 52612 Measured at 10°C (50°F) mean temperature	@ 1 mbar [2] @ ambient pressure	0.0037 0.019
Heat resistance [1] (Caused by film weld seam) (°C)		-50 <T< 120
Maximum film projection (mm)		150
Interior pressure (As delivered) (mbar)		≤ 5
Theoretical pressure rise [2] at 23°C/50% r.H. and panel thickness 20 mm (mbar/a)		~1.0
Maximum panel dimensions (mm)	Length mm Width mm Thickness mm	300 - 1200 300 - 1000 10 - 50
Length tolerances (mm)	300 to 500 mm 501 to 1000 mm 1001 to 1200 mm	+ 4.0 / -4.0 + 5.0 / -5.0 + 6.5 / -6.5
Width tolerances (mm)	300 to 500 mm 501 to 1000 mm	+ 4.0 / -4.0 + 5.0 / -5.0
Thickness tolerances (mm)	≤20 mm >20 mm	± 1.0 + 1.0 / - 2.0
Thermal shock resistance		The core material of VACUPOR® MS is insensitive to high and low temperature thermal shocks.

The above data are only intended as a guide and should not be used in preparing specifications.

Please note:
Vacupor® MS is not approved by the German building and construction authorites for building applications. Vacupor® MS may just be applied in areas where a Vacuum Insulation Panel is treated as an unregulated construction product, if an admission on a single case exists or will be obtained. The thermal conductivity value just describes the value of the Vacuum Insulation Panel under the mentioned conditions, measured in the center of the panel. The measured value does explicitly not correspond with the rated value, determined by the DIBt and may not be used in Germany for the implementation of thermal calculations for buildings.

(1) The limits are fixed by the barrier film (sealing material) used; constant load: ≤80°C (176°F); short load time with 120°C (248°F): roughly 30 minutes.
(2) According to EMPA test report No. 437840/1 dated 21st December 2006. For sample size 1000x600 mm.

Thermal conductivity
Thermal Conductivity as a function of internal pressure.

Gas Pressure (hPa)	U value (W/m²K)	λ (10^{-3} W/m·K)
$<10^{-3}$	0.187	3.63
0.1	0.188	3.66
1.0	0.193	3.75
10	0.219	4.25
150	0.448	8.70
1000	0.943	18.30

Contact

Europe:
Telephone:
+44 (0) 151 334 4030

E-mail:
marketing.tc@morganplc.com

North America:
Telephone:
+1 (706) 796 4200

E-mail:
northamerica.tc@morganplc.com

South America:
Telephone:
+54 (11) 4373 4439

E-mail:
marketing.tc@morganplc.com

Asia:
Telephone:
+65 6595 0000

E-mail:
asia.mc@morganplc.com

Porextherm:
Porextherm
Dämmstoffe GmbH
Heisinger Straße 8/10
D-87437 Kempten

Telephone:
+ 49 (0)831 - 575360
Fax:
+ 49 (0)831 - 575363

E-mail:
info@porextherm.com

Morgan Advanced Materials

POREXTHERM

Data sheet

VACUPOR® MS

Thermal Conductivity as a function of internal pressure (DIN 52612)

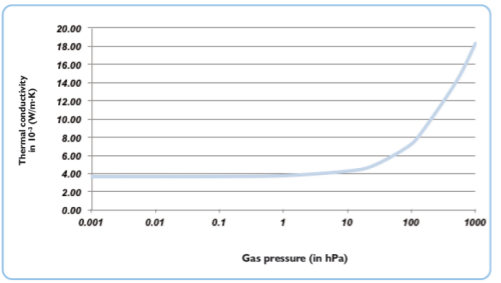

Thermal Conductivity (Panel Core) DIN 52612

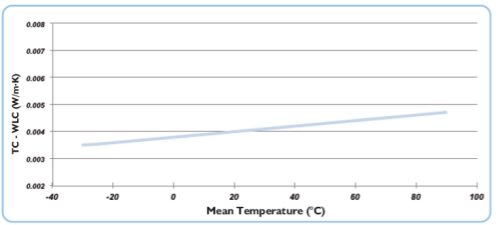

Compression Behaviour (Panel Core)

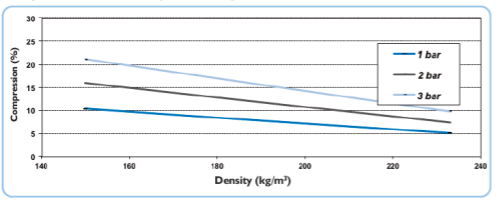

Low-temp. Compression Strength

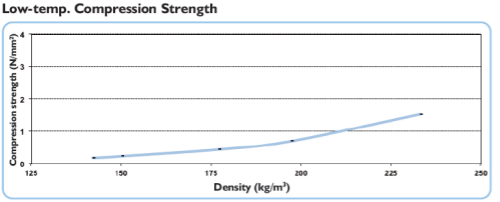

Contact

Europe:
Telephone:
+44 (0) 151 334 4030

E-mail:
marketing.tc@morganplc.com

North America:
Telephone:
+1 (706) 796 4200

E-mail:
northamerica.tc@morganplc.com

South America:
Telephone:
+54 (11) 4373 4439

E-mail:
marketing.tc@morganplc.com

Asia:
Telephone:
+65 6595 0000

E-mail:
asia.mc@morganplc.com

Porextherm:
Porextherm
Dämmstoffe GmbH
Heisinger Straße 8/10
D-87437 Kempten

Telephone:
+ 49 (0)831 - 575360
Fax:
+ 49 (0)831 - 575363

E-mail:
info@porextherm.com

Appendix II - Fiberglass VIP Datasheet

PRODUCT BROCHURE

ADVANC-R® TAKE-OFF

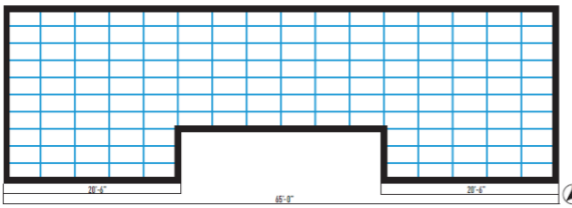

ADVANC-R®

VACUUM INSULATION PANEL

Engineered by Panasonic as the Ultra-Insulation for the building industry and tested to ASTM C1484 Standards

PRODUCT DESCRIPTION: Panasonic ADVANC-R® Vacuum Insulation Panel (VIP) is Ultra-Thermal Insulation with industry top class Center of Panel R-value of 66[1]. ADVANC-R® VIP's R-value is as high as 16.8 times that of traditional insulation[2]. ADVANC-R® is your solution to meet increasing R-value requirements, while minimizing your roofing system's profile and maximizing building space. ADVANC-R® is thin, rigid, and non-structural. ADVANC-R® is Class A rated for flame and smoke.

KEY FEATURES

- **INDUSTRY TOP CLASS CENTER OF PANEL R-VALUE 66[1]**
  Integrating 18 years of Panasonic's cutting-edge VIP technologies to engineer the Ultra-Insulator for building applications
- **SOLUTION FOR RE-ROOFING WITH HEIGHT LIMITATIONS**
  An innovative and cost effective re-roofing solution that significantly increases roofing system's R-value while minimizing the system's profile
- **INTERNAL SPACE MAXIMIZER FOR NEW CONSTRUCTION**
  Using industry top class R-value ADVANC-R® users can maximize the building's internal space by significantly reducing the roof system's profile
- **INTERTEK ETL LISTED (CONTROL NUMBER: 5011721)**

ASTM C1484	ASTM C1667
ASTM E84	ASTM C1363
ASTM C165	ASTM D2126

- **MADE OF NON-TOXIC AND ENVIRONMENTALLY FRIENDLY MATERIALS**
  Consists of 100% non-toxic materials, of which over 80% (by weight) is made from recycled materials
- **AVAILABLE SIZES:**

P/N	W x L x T (inch)	W x L x T (mm)
TZC3500E	22.4 x 24.0 x 0.94	570 x 610 x 24
TZC3490E	22.4 x 48.0 x 0.94	570 x 1220 x 24

PRODUCT SPECIFICATIONS

PART NUMBER	R-VALUE CENTER OF PANEL[1]	WIDTH		LENGTH		THICKNESS		WEIGHT		AREA		PANELS PER PALLET
	$FT^2F\text{-}H$ / BTU	IN	MM	IN	MM	IN	MM	LB	KG	FT^2	M^2	
TZC3500E	66	22.4	570	24.0	610	0.94	24	5.2	2.3	3.74	0.35	66
TZC3490E	66	22.4	570	48.0	1220	0.94	24	10.2	4.6	7.49	0.70	33

Panasonic

Panasonic Industrial Devices Sales Company of America, Division of Panasonic Corporation of North America
2 Riverfront Plaza, 7th Floor, Newark, NJ 07102-5490
• na.industrial.panasonic.com/building • building@us.panasonic.com • +1-201-392-4244 or +1-800-344-2112

PRODUCT BROCHURE

Panasonic

ADVANC-R® VACUUM INSULATION PANEL

APPLICATIONS

- ADVANC-R® is your answer to achieving higher R-value requirements, especially in re-roofing situations, where there are space constraints preventing a thicker roof profile

  - Re-roofing of commercial buildings
  - New commercial building roofs
  - Residential building with limited slopes

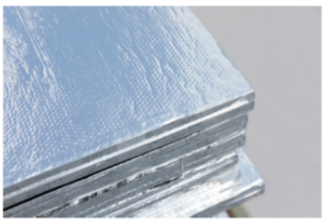

PRODUCT COMPOSITION

- Panasonic's ADVANC-R® VIP is comprised of a highly porous glass wool structure, absorbents and adsorbents in a vacuum sealed aluminum laminated bag

- The vacuum drastically reduces the transfer of heat through VIP. Our patented Fiber Layer Arrangement Technology (FLAT) radically improves thermal performance by aligning the glass wool to significantly reduce thermal conductivity by 60% (vs. conventional random orientation)

Glass Wool Orientation Effect on Thermal Conductivity

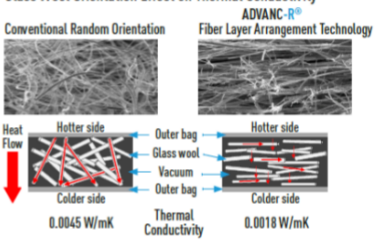

STANDARDS AND APPROVALS

- Intertek ELT: Control Number (CN) 5011721

- ASTM C1484: Super-Insulation Standards

- Factory Mutual 4470: Single-Ply, polymer-Modified Bitumen Sheet, Built-Up Roof (BUR) and Liquid Applied Roof Assemblies for use in Class 1 and Noncombustible Roof Deck Construction

- ADVANC-R® VIP is manufactured in facilities with:

  - OHSAS 18001: 2007 Occupational Health & Safety Management Systems
  - ISO 9001: 2015 Quality Management Systems
  - ISO 14001: 2015 Environmental Management Systems

CATEGORY	VALUE	TEST
Flame Spread Index[1]	Class A (15)	ASTM E84
Smoke Development Index[1]	Class A (10)	
Density[1]	13.9 lbs/ft^3	ASTM C1667
Compressive Strength @ 25%[1]	14.3 PSI	ASTM C165
Thermal and Humid Aging (after 2 weeks) [1]	7.43%	ASTM D2126
Service Temperature	-40˚F to 140˚F / -40˚C to 60˚C	

Panasonic

ADVANC-R® VACUUM INSULATION PANEL

PRODUCT HANDLING

- The outer bag of ADVANC-R® must not be damaged or compromised such that it loses its vacuum
- Neither sizes can be changed or modified
- Read ADVANC-R® Handling & Installation guidelines for more details

ROOF TAKE-OFF

- For information on optimizing ADVANC-R® layouts for commercial building roofs, please contact Panasonic Building Products and Materials Team

+1-201-392-4424
+1-800-344-2112
building@us.panasonic.com

INSTALLATION

- For commercial roofs, we recommend inserting ADVANC-R® between protective layers such as traditional insulation products (polyiso, EPS, or other similar products) or commercial gypsum roofing products
- In order to maximize R-value, we recommend staggering the seams of each layer of the roofing system
- Only use Roofing System Manufacturers approved adhesives to attach our ADVANC-R® to other layers of the roofing system. Do not use fasteners, screws, nails, staples, etc
- Stepping on the VIP may compromise the outer bag
- Ensure no foreign or sharp objects (burrs, metal shavings, screws, nails, etc) touch the ADVANC-R®
- Read ADVANC-R® Handling & Installation guidelines for more details

COMMERCIAL ROOFING INSULATION: R-Value